Journal of
Materials Chemistry A

Materials for energy and sustainability

Accepted Manuscript

This article can be cited before page numbers have been issued, to do this please use: K. Guo, A. Baidak and Z. Yu, *J. Mater. Chem. A*, 2020, DOI: 10.1039/D0TA06742C.

ROYAL SOCIETY OF CHEMISTRY

rsc.li/materials-a

View Article Online
DOI: 10.1039/D0TA06742C

Recent Advances in Green Synthesis and Modification of Inorganic Nanomaterials by Ionizing and Non-Ionizing Radiations

Kun Guo[a]*, *Aliaksandr Baidak*[b,c] *and Zhixin Yu*[d]*

[a] Institute of New Energy, School of Chemistry and Chemical Engineering, Shaoxing University, Shaoxing 312000, China

[b] Department of Chemistry, The University of Manchester, Manchester M13 9PL, United Kingdom

[c] Dalton Cumbrian Facility, The University of Manchester, Westlakes Science Park, Moor Row CA24 3HA, United Kingdom

[d] Department of Energy and Petroleum Engineering, University of Stavanger, 4036 Stavanger, Norway

Corresponding Authors

Kun Guo, E-mail: kun.guo@usx.edu.cn

Zhixin Yu, E-mail: zhixin.yu@uis.no

View Article Online
DOI: 10.1039/D0TA06742C

Abstract

Alternative to conventional Joule heating, radiation in the forms of electromagnetic waves and particle beams offers a promising route to energize the green synthesis and modification of nanomaterials with high time efficiency, simplicity, scalability, and environmental friendliness. Fundamental interactions between the atoms/molecules and the photons/high-velocity particles lead to several radiation effects that pave the way for chemical reactions and physical processes. Here, a comprehensive review is provided to summarize numerous studies concerning radiation-induced synthesis and modification of metals, metal compounds and carbon materials. We cover both ionizing and non-ionizing radiations of the full spectrum of electromagnetic waves and subatomic particle beams. The former includes γ- and X-ray, electron beam, neutron beam, and other high-energy particle beams, while the latter consists of ultraviolet, visible light, infrared, and microwave radiations. Depending on energy and intensity of the radiation source, we formulate distinct radiolysis, photolysis, knock-on, and photothermal effects that mediate the synthesis and modification. Emphasis is placed on the on-demand utilization of radiation and the fine control of structural parameters (size, composition and dispersity) of resulting materials. Lastly, we propose improvements for the novel design and implementation of radiation techniques to synthesize and modify advanced inorganic nanomaterials.

Keywords: radiation, synthesis, modification, inorganic, nanomaterials

View Article Online
DOI: 10.1039/D0TA06742C

1. Introduction

The past decades have witnessed the burgeoning applications of nanotechnology in various fields of catalysis, biomedicine, electronics, sensors, energy and so forth.[1, 2] Advancement of nanotechnology at both scientific and industrial scales is barely achievable without the workhorse of nanomaterials. Compared to the bulk counterparts, materials downsized to the nanoscale often exhibit distinct properties that in return are tightly related to their synthesis and modification at the beginning. Strategies of nanomaterial synthesis have been generalized as top-down and bottom-up methods. Physical top-down processes suffer from the poor size control of nanomaterials when breaking down the bulk materials. In contrast, chemical bottom-up methods have demonstrated the eminent superiority in the on-demand synthesis of nanomaterials with tailor-made structures, especially the wet-chemical synthetic methods.[3-5] In addition to the synthesis, modification of nanomaterials in the form of defect engineering, doping and grafting is attainable by both physical and chemical methods.

Wet-chemical synthesis involves the reactions of ions and/or the assembly of atoms in a liquid phase to generate nanomaterials.[6] To facilitate the processes, heating apparatus is often used to supply Joule heating as temperature is a crucial kinetic factor. However, severe heat dissipation occurs when large temperature gradient exists between the heat source and the ambient environment. Thermal treatment thus can be lengthy and tedious owing to the low electrical-to-thermal energy conversion efficiency. Furthermore, wet-chemical methods in many cases produce nanomaterials capped by stabilizing agents of surfactants/ligands that are subsequently daunting to remove.[7] Excessive reductants/oxidants are also added to guarantee the complete conversion of precursors. Needless to say, undesirable by-products from the synthesis cause additional issues. In

View Article Online
DOI: 10.1039/D0TA06742C

view of these deficiencies, conventional wet-chemical synthesis does not strictly meet the requirements of green, sustainable chemistry.

Radiation describes the energy emission or transmission by means of electromagnetic waves or particle beams. In daily life and real space, radiation is ubiquitous, accounting for such basic questions as why the planet Earth is habitably warm, why human eyes discern colors and how a microwave oven works. Radiation sources act as reservoirs of energy, where the energy is released in the forms of fundamental carriers of photons and particles. In sharp contrast to the heat transfer mechanism by Joule heating, photons and particles are capable of direct interaction with the atoms and/or molecules of a substance, causing a sequence of distinctive radiation effects depending on the carrier energy.[8, 9] For example, ionizing radiation of atoms and molecules generates cations/holes and escaped electrons through ionization, and free radicals through electronic excitation. Absorption of visible light could produce electron–hole pairs from photoinitiators. Microwave induces rotational transition of molecules due to the oscillating magnetic and electric fields. Utilization of these effects offers alternative approaches to synthesize and modify inorganic nanomaterials with remarkable advantages. Specifically, radiation-induced active species through radiolysis or photolysis can substitute common reductants/oxidants as *in-situ* reagents that initiate the desired chemical reactions. Energetic particles are known to induce knock-on effect in the irradiated target, resulting in the introduction of defects and doping to the material. Thermal shock by transient microwave absorption rapidly elevates the local temperature to over 1000 K, allowing substantial reduction of the temporal scale from hours for conventional synthesis to seconds for microwave-assisted synthesis. Recently, a growing number of studies have reported the green synthesis and modification of inorganic nanomaterials driven by radiation and revealed the great potential of this strategy.

View Article Online
DOI: 10.1039/D0TA06742C

Despite that several reviews have already summarized the material synthesis/modification using certain types of radiation, a systematic and comprehensive review covering the full spectrum of electromagnetic waves as well as the particle beams is still lacking.[10-18] Since radiation effects strongly rely on the specific radiation source, it is thus crucial to provide a panoramic view of their respective strengths and limitations so that creative and innovative utilization of radiation could be inspired. To this end, we here summarize recent advances in radiation-induced synthesis and modification of inorganic nanomaterials inclusive of metals, metal compounds and carbon materials. These materials are chosen as they constitute a major part of the inorganic materials and have shown intriguing properties for a variety of applications.[19-30] The outline of this review is illustrated in Fig. 1. This review starts by summarizing radiation effects that are applicable in the green synthesis and modification. Next, in-depth discussion is conducted on the radiation techniques grouped into ionizing and non-ionizing. The former includes γ-ray, X-ray and high-energy particle beam, while the latter consists of ultraviolet (UV), visible light, infrared (IR), and microwave. Underlying mechanisms of these radiation techniques, generalized as radiolysis, photolysis, knock-on, and photothermal effects, are formulated. Critical parameters to finely regulate the product size, composition and distribution are pinpointed. It is then followed by contemplating promises and challenges of these radiation techniques. Note that we concentrate on the radiation-induced chemistry and its corresponding exploitation, whereas the physical phenomena is left outside the scope of this review.

View Article Online
DOI: 10.1039/D0TA06742C

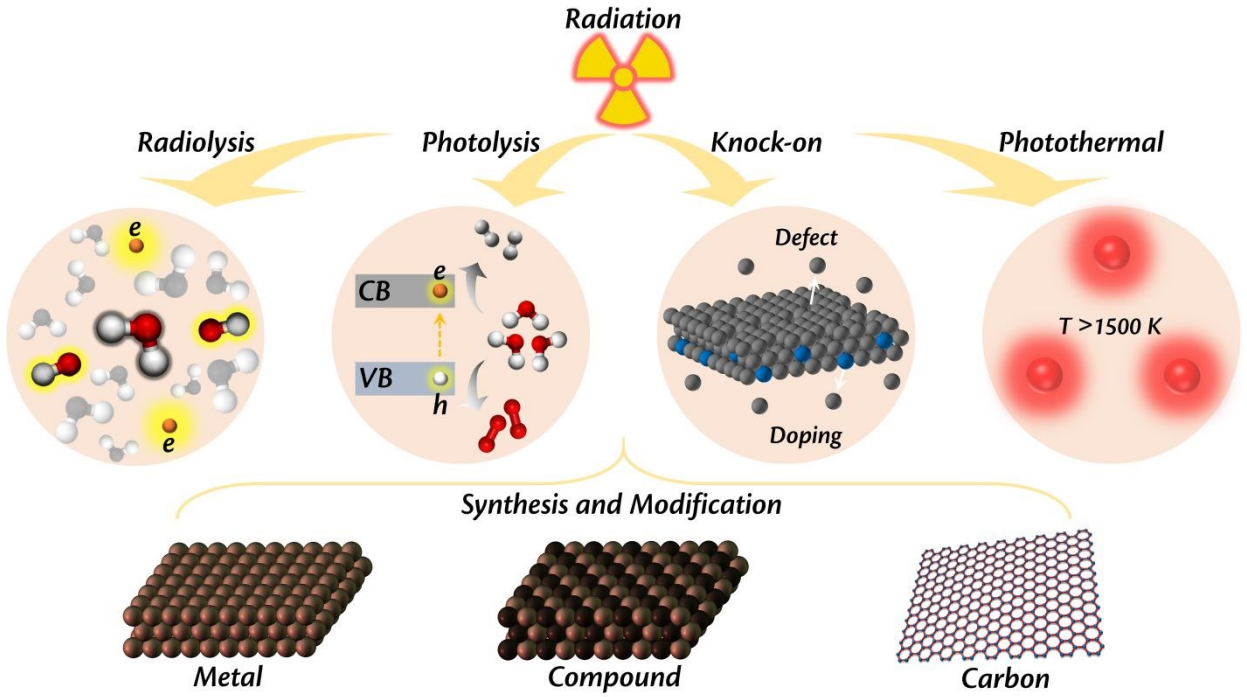

Fig. 1 Schematic illustration of radiation-induced synthesis and modification of metals, compounds and carbon materials through four major mechanisms of radiolysis, photolysis, knock-on, and photothermal effects, depending on the nature of radiation source.

2. Theoretical Background

2.1. Radiation Effect

When a substance is exposed to a radiation source, the radiation effect can be at atomic, molecular and/or bulk scale depending on the radiation energy. Fig. 2 illustrates six common effects resulted from the electromagnetic and particulate radiations. *Atom ionization* refers to the phenomenon when one or more electrons are ejected as free electrons from atoms/molecules. The ejected electrons can come from either core or shell electrons. This ionization effect is observed for such radiations as α-, β-, and γ-rays, and hard X-rays that possess sufficiently high photon energy to overcome the electron binding energy. If the radiation energy is smaller than the electron binding energy (like soft X-rays), core electrons absorb the incident photon energy and jump to higher energy levels, resulting in the *electron transition*. In the case of a molecule being irradiated, its

View Article Online
DOI: 10.1039/D0TA06742C

molecular structure plays a decisive role in the radiation effect. For example, polar molecules tend to be ionized with the formation of electron-hole pairs, whereas non-polar molecules mostly go through electronic excitation (from low-energy orbitals to high-energy orbitals) that leads to *bond breaking* since chemical bonds are essentially interactions between electron orbitals. As the radiation energy further decreases to the electromagnetic spectrum range of UV, visible light and IR, the photon energy becomes comparable to molecular electronic energy and phonon energy. Absorption of such photon energy then gives rise to the *molecular transition* and *vibrational transition* that can induce photochemical reactions with the generation of active radicals. Further down to the microwave range, the *rotational transition* of polar molecules could be triggered, which for instance generates photothermal effect. Note that despite the above-mentioned radiation effects, only part of them can actually be utilized for material synthesis and modification.

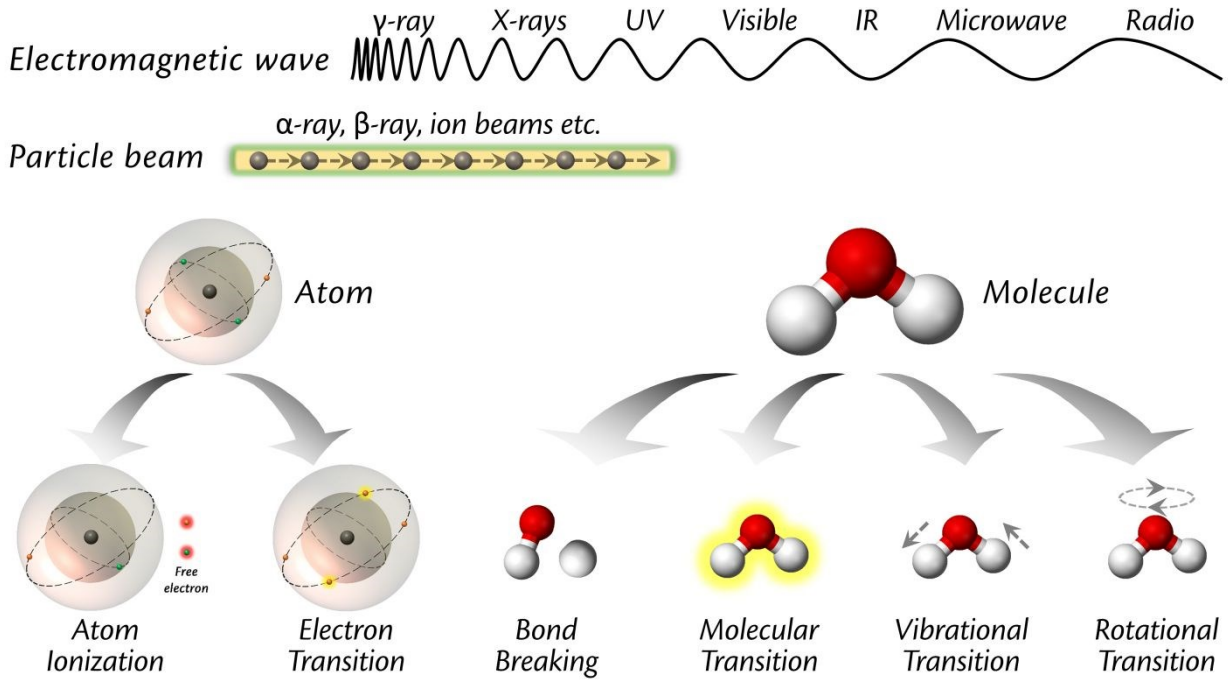

Fig. 2 Schematic illustration of two types of radiation sources (electromagnetic wave and particle beam) and radiation effects on representative atoms and molecules. Correlated to energy and intensity of the radiation source, six common radiation effects, including atom ionization, electron transition, bond breaking, and molecular, vibrational and rotational transitions, can be produced on atoms and molecules.

View Article Online
DOI: 10.1039/D0TA06742C

2.2. Ionizing Radiation

Self-evidently, ionizing radiation defines a radiation that can dismiss electrons from atoms or molecules, that is, ionize them. Such radiations can be electromagnetic waves or particle beams whose photon energy is high enough to surmount the electron binding energy. Table 1 details the common categorization of electromagnetic spectrum according to its wavelength and photon energy. Electromagnetic waves in the spectrum range of γ-rays, X-rays and high-frequency UV that readily ionize atoms or molecules belong to ionizing radiations. Among them, γ-rays are known to be the most energetic and penetrating electromagnetic wave that can cause deadly harm to human bodies. In addition, high-energy particle beams made of subatomic particles (protons, electrons and positrons that carry positive/negative charges, or neutral neutrons) and ions (α particles) are also grouped into ionizing radiations. The charged particles come from either the radioactive decay or the acceleration to a high velocity by applying a high-voltage electric field. Generation of ionizing radiations requires sophisticated instruments and the operation warrants professional training to protect the users.

Table 1 Common categorization of the electromagnetic spectrum into γ-ray, X-ray, UV, visible light, IR, and microwave radiations based on the wavelength and photon energy.

Category	Subcategory	Wavelength (nm)	Photon Energy (eV)
γ-ray		$< 10^{-3}$	$> 1.24\times10^{6}$
X-ray	Hard X-ray	10^{-3}–10^{-1}	1.24×10^{4}–1.24×10^{6}
	Soft X-ray	10^{-1}–10	124–1.24×10^{4}
UV	Extreme UV	10–121	10.2–124
	Far UV	122–200	6.2–10.2
	Middle UV	200–300	4.1–6.2
	Near UV	300–400	3.1–4.1
Visible light		400–700	1.8–3.1
IR	Near IR	700–1.4×10^{3}	0.89–1.8

View Article Online
DOI: 10.1039/D0TA06742C

	Middle IR	1.4×10^{3}–3×10^{3}	0.41–0.89
	Far IR	3×10^{3}–10^{6}	1.2×10^{-3}–0.41
Microwave		10^{6}–10^{9}	1.2×10^{-6}–1.2×10^{-3}

2.3. Non-Ionizing Radiation

In contrast, non-ionizing radiations have lower photon energy than ionizing radiations. Such radiations excite electrons or molecules to higher energy states (molecular transition) and cause molecular vibration and rotation. Excitement of electrons or molecules leads to photochemical reactions with the production of active free radicals. On the other hand, molecular vibration and rotation are often translated with the emission of thermal energy. Examples of non-ionizing radiation are in the electromagnetic spectrum range of low-frequency UV, visible light, IR, and microwave (**Table 1**). Note that in the spectrum of electromagnetic wave, there is no clear dividing line between ionizing and non-ionizing radiations. Although the single photon may not be able to ionize atoms or molecules, multiple photons of lower energy can still take effect collectively and lead to the ionization of atoms and molecules, especially in the cases of UV and visible lights. Contrary to ionizing radiation, sources of non-ionizing radiation are more ubiquitous, less costly and less hazardous. Therefore, it is much easier to have routine access to non-ionizing radiation than ionizing radiation in the laboratory.

2.4. Terminology

2.4.1. Photon Energy and Intensity

To quantify the energy of a radiation, especially an electromagnetic wave, its photon energy symbolized by E is a straight-forward measurement. In quantum physics, photon energy E equals to the product of the Planck constant h and the photon's frequency v, in which frequency v is the quotient of the speed of light c and the photon's wavelength λ. Photon energy E can be expressed

View Article Online
DOI: 10.1039/D0TA06742C

in the unit of electron volt (eV) or joule (J). For example, γ-rays are regarded to have photon energies in the magnitude of 10^2 keV and above. X-rays have photon energies between 10^{-1} and 10^2 keV. Whereas the photon energies of visible light are in the range of 1.7–3.3 eV. Upon radiation, the resulting effects are not only related to the energy of individual photon, but also to the quantity of emitted photons per unit time and area, which is designated as radiation intensity. The photon energy may be insufficient to ionize a molecule, but can be sensed as thermal radiation. With more photons received, the accumulation of thermal energy can ultimately surpass the energy barrier and thereby lead to ionization.

2.4.2. Radiolysis and *G*-value

Analogous to electrolysis and photolysis, radiolysis describes the process in which the molecules are dissociated by radiation. Radiolysis of a substance is complex. The radiolytic products can be a combination of subatomic particles, free radicals, ions, and molecules. To quantify such radiolytic products, researchers adopted the concept of *G*-value, which is defined by the number of molecules, atoms or free radicals yielded (or consumed) per 100 eV of energy absorbed by the substance. Of all the substances, water radiolysis is the most well-established, as shown in Eq (1) where the *G*-values are in parentheses.[31, 32]

$$H_2O \xrightarrow{radiation} e_{aq}^{-}(2.7), HO^{\bullet}(2.8), H^{\bullet}(0.6), H_3O^{+}(2.7), H_2(0.47), H_2O_2(0.75) \quad (1)$$

Eq (1) tells that both reducing and oxidizing species are generated during the radiolysis of water. Such active species have been widely used to reduce metal precursors or oxidize carbon surface in the presence of suited scavengers for the detrimental species. For instance, small alcohols are effective to scavenge the oxidizing hydroxyl radicals ($HO^{\bullet}$), while N_2O is useful to neutralize the reducing e_{aq}^{-} species.

View Article Online
DOI: 10.1039/D0TA06742C

2.4.3. Absorbed Dose and Dose Rate

In view of the radiolysis, the energy absorbed by a substance with a specific mass needs to be calculated to measure the quantity of radiolytic products. In dosimetry, this energy is quantified using absorbed dose, which measures the absorbed energy by a substance per unit mass. The SI (International System of Units) base unit of dose is gray (Gy). 1 Gy equals to 1 joule of energy absorbed per kilogram of matter (1 Gy=1 J kg^{-1}). On a temporal scale, dose rate further describes the time needed to deliver a specific dose to a substance. The SI unit of dose rate is Gy s^{-1}. Both absorbed dose and dose rate are considered important kinetic parameters since they directly determine the concentration and total amount of generated active species in the course of synthesis/modification.

3. Ionizing Radiation

3.1. γ- and X-Ray Irradiation

γ- and X-ray are essentially made of high-energy photons. γ-ray arises from the radioactive decay of atomic nuclei, such as ^{60}Co and ^{137}Cs sources. Whereas, X-rays are emitted whenever charged particles of sufficiently high energy, such as electrons and ions, hit a substance. Notwithstanding the radiation risks, it does not stop researchers from arousing immense interests in utilizing γ- and X-ray for the synthesis and modification of various materials. Prominent advantages of such ionizing radiations are the easiness, low cost and zero emission. One just needs to place the stock solution inside the irradiator chamber, set the radiation parameters and then wait it out to receive the final products. Since γ-ray is generally more energetic and penetrating than X-ray, utilization of γ-ray in the synthesis and modification is thus even more intriguing. In the following subsections, synthesis and/or modification of metals, compounds and carbon materials are summarized.

View Article Online
DOI: 10.1039/D0TA06742C

3.1.1. Metals

Preparation of metallic nanoparticles (NPs) can be traced back to the pioneering study reported by Yamazaki and colleagues in 1960s.[33] The authors observed the formation of a gold particle-containing gel when an aqueous solution of chloroauric acid was irradiated with γ-rays from a ^{60}Co source. Later, mono- and bi-metallic NPs were also prepared by γ-ray irradiation of an aqueous solution with metal precursors.[34-37] Since then, considerable attempts have been made in exploring the utilization of radiation to prepare metallic NPs.[38-52] Simplified mechanism of high-energy radiation-induced synthesis of monometallic NPs is illustrated in Fig. 3. A degassed container with an aqueous solution of metal precursor is irradiated. Metal cations are gradually reduced to metal atoms by reducing species generated from the radiolysis of H_2O. Meanwhile, oxidizing species from H2O radiolysis are scavenged by alcohol molecules, such as isopropanol (IPA). Driven by the supersaturation, metal atoms then start to coalesce to form small nuclei. If the size of a nucleus exceeds the critical radius, the nucleus grows into larger sizes by combining more atoms, otherwise it dissolves into smaller sizes or merges with other larger clusters. To stabilize the metal NPs from further growing or Ostwald ripening, surfactants and/or supporting materials are often introduced prior to the radiation to obtain surfactant-protected and/or supported NPs. No electric heating or mechanical mixing is applied.

View Article Online
DOI: 10.1039/D0TA06742C

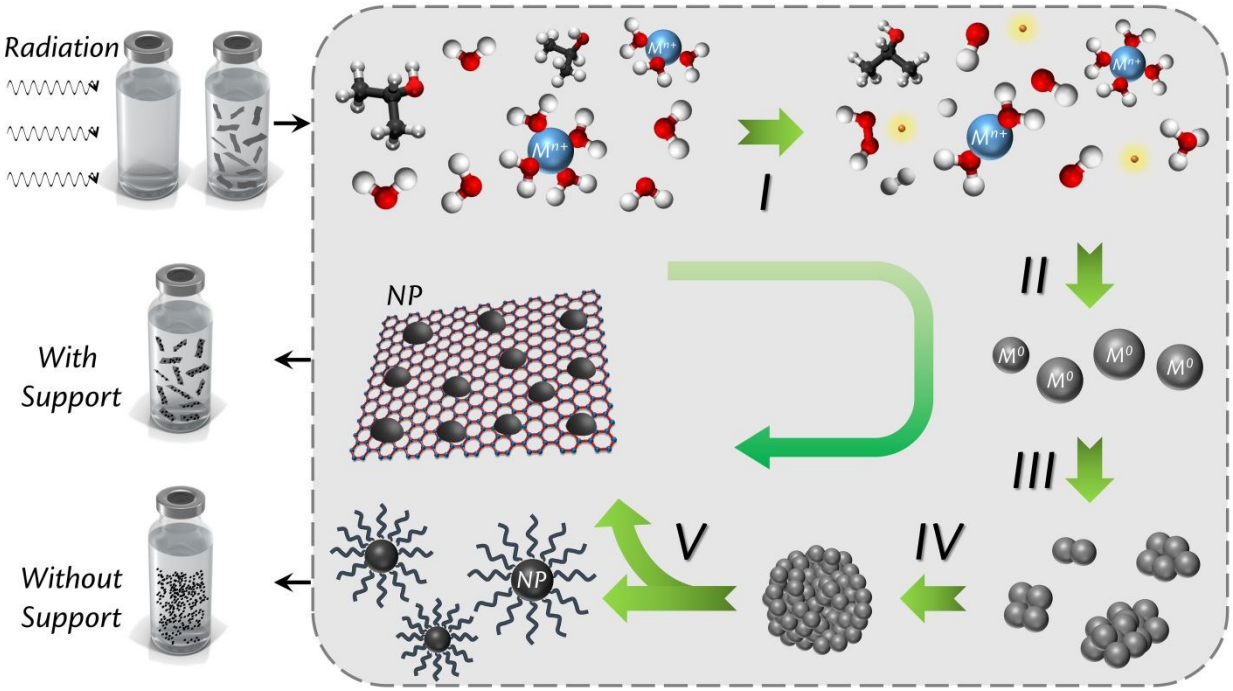

Fig. 3 Schematic illustration of the synthesis of supported and unsupported metal NPs in an aqueous solution with/without pre-existing supports (exemplified by graphene support) using high-energy radiation. The synthesis consists of five representative steps of (I) absorption of radiation and formation of reactive species, (II) cation reduction, (III) nucleation, (IV) growth, and (V) stabilization. H_2O, IPA, H_2O_2, and H_2 molecules, hydrated cations, $OH^{\bullet}$ and $H^{\bullet}$ radicals, solvated electrons, H_3O^+ ions, metal atoms, clusters and NPs, surfactant and graphene support are illustrated. The NPs are anchored on the support surface or stabilized by surfactant molecules.

As a straightforward method, the radiation-induced synthesis often leads to the formation of spherical metal NPs. Therefore, the main objective, in most cases, is to control the size and dispersity of the NPs, which are affected by several factors inclusive of solvent, cation concentration, dose, dose rate, surfactant and support. Table 2 and 3 summarize the detailed synthetic parameters for the γ- and X-ray radiation-induced synthesis of metal NPs in the presence of surfactant and support, respectively. Water is by far the most widely-used solvent due to the well-established radiolysis of water. In addition to water, a small fraction of alcohol, such as IPA and methanol, is added as a scavenger of the oxidizing species generated from water radiolysis. Note that IPA molecules also generate a considerable amount of reducing radicals once reacted with those oxidizing species. Distinct from conventional colloidal synthesis in which an external

View Article Online
DOI: 10.1039/D0TA06742C

reductant is added intentionally, the reductants in the radiation-induced synthesis are *in-situ* generated from the stock solution at a constant speed that is determined by the dose rate.

Table 2 Summary of the synthetic parameters for γ- and X-ray radiation-induced synthesis of metal NPs in the presence of surfactants.

Type	Metal	Stock Solution				Radiation Parameters		Particle Size[b] (nm)	Ref.
		Volume (mL)	[Metal] (mM)	Solvent	Surfactant[a]	Dose (kGy)	Dose Rate (Gy s^{-1})		
γ-ray	Ir	20	5	H_2O-IPA	SDS	60	1.94	2.3	53
	Au	—	0.5	H_2O-IPA-acetone	PVP	1.7	0.61	6–13	54
	Ag	1000	29	H_2O-IPA	PVP	10–30	0.28	(24–39)	55
	Ag	—	0.74–1.84	H_2O-IPA	PVP	10–70	—	(15–70)	56
	Ag	5	30	H_2O-IPA	PVP	0.5–4	0.28	(15–60)	57
	Ag	50	6.5	H_2O	PVP	150	0.75	(11–20)	58
	Au	26–30	0.1–1	H_2O-methanol	PEGDMA	15	0.58–1.33	(8–35)	59
	Au	10	0.729	H_2O	NIPAM	192	0.83	(7.18)	60
	Cu	—	5–15	H_2O	PVA	100–300	—	(13.9–19)	61
	U	12.5	4	H_2O-methanol	PVA, citrate	7.56	3.5	(~6)	62
	ULa(Eu)	12.5	4	H_2O-methanol	PVA, citrate	7.56	3.5	(~2)	
	AlCu	—	50–64	H_2O-IPA	PVP	80–120	0.81	(4.5–12)	63
	AlNi	—	0.05–0.064	H_2O-IPA	PVA	100	—	(4.43–9.97)	64
	Ag_xNi_{1-x}	50	0.2	H_2O-methanol	PVA, citrate	3.24	3	(3.4–8.5)	65
	$Pd_{0.5}Ni_{0.5}$	50	0.2	H_2O-methanol	PVA, citrate	6.48	3	5.1–6.8	
X-ray	Au	—	2	H_2O-IPA	urea	7.26		(1.1)	66
	Au	—	1	H_2O-IPA-acetone	polypeptide	1	0.25	10–20	67
	Cu	—	—	H_2O-ethanol	PAA, PEI	108	20	15–20, 1–3	68
	Ag	—	—	H_2O-ethanol	PAA, PEI	18	20	2–6	

[a] Abbreviations: SDS = sodium dodecyl sulfonate, PVP = polyvinyl pyrrolidone, PEGDMA = polyethylene glycol dimethacrylate, NIPAM = *N*-isopropylacrylamide, PVA = polyvinyl alcohol, CTAB = cetyltrimethylammonium bromide, PAA = polyacrylic acid, PEI = polyethylenimine.

[b] The particle size refers to the size range of NPs, whereas in parentheses are the average particle sizes (APSs) or the range of APSs at varied synthetic conditions.

Table 3 Summary of the synthetic parameters for γ- and X-ray radiation-induced synthesis of metal NPs in the presence of supports.

Type	Metal	Stock Solution				Radiation Parameters		Particle Size[b] (nm)	Ref.
		Volume (mL)	[Metal] (mM)	Solvent	Support[a]	Dose (kGy)	Dose Rate (Gy s^{-1})		
γ-ray	Pd	12	5.6	H_2O-IPA	MWCNT, SDS	10–40	2.78	(4–11, 32–47)	69
	Pt	10	0.25	H_2O-IPA	SiO_2	1.6	0.08	3–5	70
	Pt	10	0.25	H_2O-IPA	MWCNT	1.6	0.08	< 10	71
	Au	—	0.248	IPA	SnO_2	20	2.78	(~60)	72
	Pt	80	1.5	H_2O-IPA	GO	200	2.78	(100)	73
	Pd, Pt, Au	5	5	H_2O-IPA	UiO-66-NH_2	18	1.67	(1–2)	74
	Ag	16.5	5.4	H_2O	GO	160	2.67	(20)	75
	Ag	—	3	H_2O-IPA	ZnO	100	0.81	(15)	76
	AgAu	4	4.2	H_2O-IPA	GO, CTAB	29	1	5–19	77
	Pd	16	250	EG	N-graphene	42	5	(3)	78
	Pt	—	2	EG	GO	300	5	(1.8)	79

[a] Abbreviations: MWCNT = multi-walled carbon nanotube, GO = graphene oxide.

[b] The particle size refers to the size range of NPs, whereas in parentheses are the APSs or the range of APSs at varied synthetic conditions.

View Article Online
DOI: 10.1039/D0TA06742C

Superiority of radiolytic synthesis relative to conventional chemical reduction has already been testified. Yu and co-workers prepared Vulcan XC72-supported Pt NPs by three different methods of γ radiation, $NaBH_4$ reduction and polyol reduction.[80] The authors found that Pt NPs prepared by γ radiation demonstrate excellent oxygen reduction activity, higher Pt utilization efficiency, and improved fuel cell performance compared to Pt catalysts prepared by conventional reduction methods as well as the commercial Pt catalyst.

To implement the radiolytic synthesis, researchers have placed much emphasis on parametric studies in terms of optimizing the radiolytic conditions to control the kinetics. Specifically, precursor concentration is an important kinetic parameter that strongly affects the ultimate NP size and dispersity. Higher concentration often results in larger size and worse dispersity because the nuclei are easier to grow with more available atoms surrounded in the solution.[81] NP aggregation would also become more severe since more NPs are formed. To fully reduce the metal cations, a threshold dose is required. The actual dose is often set beyond this threshold. Reported studies indicate that the effect of radiation dose on NP size remains controversial, as opposite results are experimentally observed by different researchers. Some reported that the particle sizes decrease with increasing dose.[55, 56, 64, 82] Yet, others found that larger dose gives larger NPs.[57, 61, 72] Moreover, the dose rate resembles the strength of a reductant. A higher dose rate endows a faster generation of metal atoms and vice versa. Higher atom concentration gives higher supersaturation, which reduces the critical nucleus size according to the classic nucleation and growth theory. Thereafter, larger amounts of nuclei with smaller sizes are formed at higher dose rates, yielding smaller NP sizes.[83, 84]

When more than one type of metal cations are present, the radiolysis principle remains the same, but the evolution of bi- and/or multi-metallic NPs depends on the dose rate and the gaps between metal redox potentials.[85-87] Metals with more negative reduction potentials are reduced first as the

View Article Online
DOI: 10.1039/D0TA06742C

cores, which are then coated by metals with more positive reduction potentials, forming core@shell structured bimetallic NPs. Metals with close reduction potentials are reduced almost concurrently, leading to homogeneous alloy NPs. On the other hand, at relatively high dose rates, a large amount of reducing species are rapidly generated. Metal cations thereby could be reduced simultaneously rather than successively, regardless of their redox potential differences. Composition-separated NPs thus would tend to form at lower dose rates.

Apart from the above kinetic parameters, surfactant and support also play an important role in controlling the NP size and dispersity. In the presence of surfactant or support, the classic nucleation and growth theory is not strictly applicable because the nuclei can adsorb surfactant molecules or adhere to support surface to reduce the surface energy. The growth stage and/or Ostwald Ripening are thus disturbed, giving relatively small NP size and good dispersity. To date, carbon materials and oxides, such as graphene, CNT, silica, and alumina, have been employed as supports. Despite the effectiveness of surfactant molecules in size control of NPs, the removal of surfactants is a long-standing challenge to recover NPs with clean surface for further applications.

The core issue of radiation-induced synthesis remains the precise engineering of NP size and dispersity. In light of this, creative attempts have been tried by coupling the concept of confinement effect. Benefiting from the large amount of micro-pores inside the zeolite and the high penetration of γ-rays, the nucleation and growth of NPs are confined within the micro-pores throughout the zeolite support, ensuring the ultrafine NP size and high dispersity.[88, 89] Similarly, water-in-oil emulsion could also be chosen to confine the NPs within the water droplets suspended in the oil phase, provided that the metal precursor solution is aqueous and would not transfer to the oil phase.[90, 91] Furthermore, alternative solvent besides water offers another potential route to control the NP size and dispersity. Guo and co-workers obtained ultrafine Pd and Pt NPs uniformly supported on N-doped graphene by irradiating a solution using ethylene glycol (EG) as the

View Article Online
DOI: 10.1039/D0TA06742C

solvent.[78] It is demonstrated that EG with moderate reducibility and higher viscosity is a superior solvent to water in the size control of NPs. Reduced GO (rGO) supported Pt NPs with an average particle diameter of 1.8 nm was also prepared in EG solvent by Zhai and colleagues.[79] These studies validate the potential of radiolytic synthesis using unconventional solvents in addition to water.

3.1.2. Metal Compounds

Following a similar route to the metals, synthesis of metal oxides or sulfides by high-energy radiation is also achievable. Such metallic elements often feature with multivalence nature and distinct solubility of cations with varied valence states. Exemplary metals include iron[92-94], cobalt[95, 96], chromium[97], and manganese[98]. The formation of metal oxides can go through a sequence of reactions. Wren and co-workers found that the formation and growth of magnetite NPs by γ radiation of $FeSO_4$ solutions constitute three kinetic stages.[92] Stage 1 involves the oxidation of soluble Fe^{2+} to less soluble Fe^{3+} by $HO^{\bullet}$ radicals, followed by hydrolysis of Fe^{3+} and the co-precipitation of Fe^{2+}/Fe^{3+} hydroxide particles. Stage 2 is represented by the surface adsorption of Fe^{2+} to existing particles and subsequent oxidation of adsorbed Fe^{2+} to Fe^{3+}. Stage 3 refers to the negligible net oxidation of Fe^{2+} in the particle coarsening. Similar results were also found by the same research group on the radiation-induced formation of Co_3O_4 NPs from aqueous $CoSO_4$ solution.[96] Furthermore, Lee and colleagues reported the radiolytic fabrication of a stable, highly-porous Prussian blue (PB)/PVP/rGO aerogel based on the different standard redox potentials of Fe^{3+}/Fe^{2+} and $[Fe(CN)_6]^{3-}/[Fe(CN)_6]^{4-}$ pairs.[99] Fe^{3+} is first reduced by radiolytic reducing species to Fe^{2+}, which is then oxidized by $[Fe(CN)_6]^{3-}$ to form PB NPs.

Radiolytic synthesis of sulfides has also been reported, but the synthetic mechanism is different from that for the oxides. Based on the radiolytic reduction of thiosulfate ($S_2O_3^{2-}$) that generates S^{2-} anions, Zhai and co-workers prepared PVP-capped CdS nanopopcorns.[100, 101] Following an analogous mechanism, the same group also reported the synthesis of carbon black supported MoS_x

View Article Online
DOI: 10.1039/D0TA06742C

from thiomolybdate anions (MoS_4^{2-}).[102] Radiolysis of EG solvent generates solvated electrons that reduce MoS_4^{2-} to MoS_x.

In addition to the synthesis, γ- and X-ray radiations have also been employed in the modification of electrical, optical and structural properties of metal compounds, especially by means of defect engineering.[103] Due to the unique electronic structure, transition metal chalcogenides (TMC) have triggered tremendous amount of attention and remain a hot spot for various research fields. When downsizing TMC from bulk to monolayer, it is found that TMC is transitioned from having an indirect band gap to a direct band gap. The photoluminescence (PL) property of TMC is thus significantly enhanced. However, the PL intensity is strongly related to the structural, mechanical and electrical properties of TMC monolayers. Huang and co-workers reported the effects of γ radiation on a WS_2 monolayer semiconductor.[104] Several radiation-induced effects that play an important role in modifying the physical properties of a WS_2 monolayer are suggested, as shown in Fig. 4. These processes include photoelectric absorption, Compton scattering, pair production, vacancies and fast electrons. The authors found that γ-ray radiation led to the creation of S and W vacancies, contributing to the change from diamagnetic to ferromagnetic property of the WS_2 monolayer. In addition, the S vacancies endowed WS_2 monolayer with higher hole concentration than electron concentration, meaning that p-type doping was introduced to the semiconducting WS_2. The doping concentration also increased substantially with the increase in radiation dose as more vacancies were created. In view of this, WS_2 monolayer is claimed to be an appealing candidate for sensing high-energy photons at small radiation doses. The potential application as an ultrasensitive detector is also reported by Feng and co-workers who demonstrated that MoS_2 resonators are robust yet sensitive to very low dosage γ-ray.[105] With respect to vacancy creation by radiation, the impact of atmosphere should not be overlooked. Park and colleagues reported the formation of S vacancies by irradiating MoS_2 films, which were found to be oxidized to MoO_x after

View Article Online
DOI: 10.1039/D0TA06742C

radiation.[106] Furthermore, Vogl and co-workers specifically investigated the effect of atmosphere on irradiated WS_2.[107] When O_2 was present, S vacancy healing was observed due probably to the chemisorption of dissociated O_2 molecules at S vacancy sites facilitated by γ-rays. Moreover, Xiang and colleagues irradiated MoS_2 materials with varied doses of 1–1000 kGy and discovered that the optical bandgap of MoS_2 increased monotonically with higher doses.[108] Changes on the electrical, optical and structural properties caused by γ-ray and X-ray radiation have also been found on TiO_2[109], In_2O_3[110], CeO_2[111], MoO_3[112], HfO_2[113], $SrZnO_2$[114], Cd_2SnO_4[115], $BaTiO_3$[116], CoS[117], ZnS[118], and ZnTe[119].

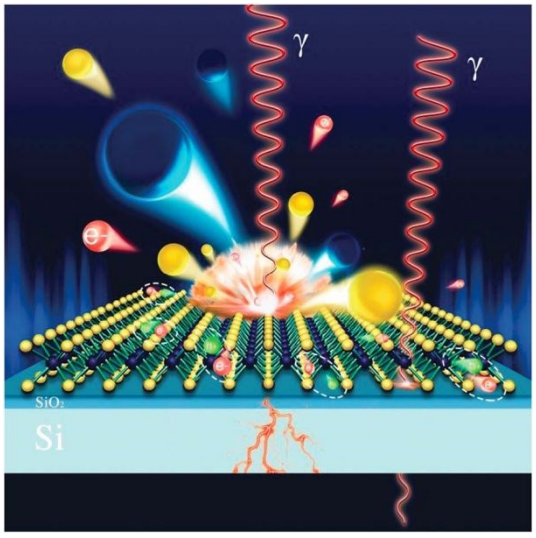

Fig. 4 Schematic illustration of the radiation effects of γ-rays on a WS_2 monolayer with the generation of secondary γ photons (in the silicon substrate), electron/hole pairs, fast electrons, and vacancies. Reproduced with permission.[104] Copyright 2020, The Royal Society of Chemistry.

3.1.3. Carbon

Carbon materials are another important branch of research objects that strongly interact with high-energy radiation. Carbon exists in the form of many allotropes inclusive of diamond, CNT, graphene, fullerene, amorphous carbon and so forth. By far, radiation effect on some of the allotropes has been reported in the forms of the modification of their physical and/or chemical

View Article Online
DOI: 10.1039/D0TA06742C

properties. Reduction/oxidation, defect engineering and surface functionalization can occur to carbon materials depending on the medium in which the materials are being irradiated.[120-124]

Park and co-workers irradiated MWCNTs by γ-rays in O_2 atmosphere in the absence of any solvent.[125] Oxygen atoms were incorporated to the surface of CNTs as oxygen-containing functional groups, which brought strong interaction between the CNTs and the polyamide 6,6. Similar results were also observed by Miao and colleagues who applied γ radiation to CNT yarns in air.[126] The authors found that the oxygen content, for instance the content of carboxyl groups, increased dramatically after irradiation treatment in air. Such oxygen groups strengthened the interaction between adjacent CNTs by forming hydrogen bonds and the mechanical properties of CNT yarns were thus improved. Xu and co-workers irradiated MWCNTs by γ radiation both in air and in epoxy chloropropane (ECP) solvent.[127, 128] Distinct radiation effects were observed in the two different media. γ radiation in air resulted in higher graphitization degree and smaller interlayer distance of CNTs, while more defects were created in CNTs that was irradiated in ECP.

Besides CNTs, two-dimensional graphene and GO are also intensively studied in terms of the radiation effects.[129] As mentioned earlier, radiolysis of water generates both reducing and oxidizing species, which can be used to reduce GO and oxidize graphene, respectively.[130-135] Li and co-workers reported the radiation-induced reduction of GO in N_2-purged water–alcohol solvent.[133] GO was successfully reduced to rGO with decreased content of oxygen functional groups, increased graphitization degree and decreased interlayer spacing. γ-ray induced reduction of GO was also reported by Zhang and colleagues using a GO suspension in *N*,*N*-dimethyl formamide.[134] The rGO could be well-dispersed in various organic solvents due to the stabilization of $N(CH_3)_2^+$ groups on its surface. Furthermore, synchronized reduction and hydrogenation of GO were reported by Yan and co-workers.[136] They discovered that rGO was simultaneously hydrogenated by hydrogen radicals formed in water radiolysis.

View Article Online
DOI: 10.1039/D0TA06742C

On the other hand, radiolytic oxidizing species can enable the modification of GO from a different perspective. To engineer porous structure on GO sheets, Li and co-workers adopted an "etching" strategy by oxidizing GO with HO• radicals generated from the radiolysis of N_2O-saturared water.[135] Carbon atoms located on the edges and basal planes of GO sheets could be removed as CO_2 or CO, forming 'lacelike' edges and nanopores in GO, as shown in Fig. 5. Compared to the pristine GO with sharp edge and flat basal plane, GO irradiated for 6 h has a rougher surface with wrinkles appearing across the whole GO sheets. When extending the radiation time to 17 and 23 h, the sharp edge turns into 'lacelike' edges and the basal pane is enriched with pores.

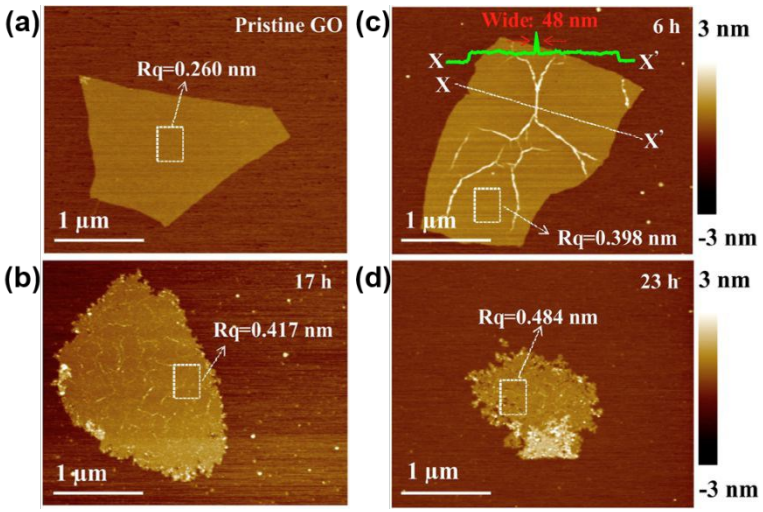

Fig. 5 Atomic force microscopy (AFM) images of GO sheets before and after γ radiation: (a) Pristine GO. (b, c, d) GO irradiated for 6, 17, and 23 h, respectively. Surface roughness (Rq) of GO sheets is indicated. Adapted with permission.[135] Copyright 2016, Elsevier Ltd.

Graphene surface functionalization is also achievable by high-energy radiation. This is often done by combining the radiation-induced reduction and graft polymerization. Radical polymerization of monomers to polymers driven by radiation has been documented for decades.[137, 138] Herein we only focus on the surface functionalization of graphene, while the polymerization mechanism will not be discussed. To prepare styrene-functionalized graphene, Xu and co-workers proposed a facile

View Article Online
DOI: 10.1039/D0TA06742C

strategy of intercalation, grafting and self-exfoliation by irradiating a suspension of GO in styrene–toluene solvent.[139] After radiation, styrene is polymerized to polystyrene and grafted to graphene sheets. The steric hindrance of polystyrene counteracts the Van der Waals forces between graphene layers. The resulting functionalized product thus contains a high amount of graphene monolayers and little agglomeration is observed. By simply changing the monomers to acrylic acid (AA), acrylamide (AM), vinyl acetate (VA), silane, and 4-vinylpyridine (4VP), researchers have also obtained functionalized GO grafted with PAA, PAM, PVA, organosilane, and P4VP.[140-143]

3.2. Particle Irradiation

Distinct from the γ- and X-rays that are essentially electromagnetic waves made up of discrete photons, particle radiation refers to a beam composed of moving particles. Such particles are either electrically charged or neutral. Apparently, the particles can interact with the irradiated target in a different pattern from the photons. To enable the atom ionization, the speed of particles needs to be very high so that the kinetic energy can surpass the ionization energy of target atoms. Conventionally, particulate ionizing radiation is represented by subatomic particle beams, including α, β, neutron and proton particles. α radiation describes a radioactive decay that gives off a particle (α particle) consisting of two protons and two neutrons, which essentially are the nucleus of a helium atom. β radiation refers to the process in which either an electron or a positron (same particle as an electron, but with a positive charge) being emitted from an atom. Albeit the widespread application of other forms of (heavy) particle radiation in materials science, such as focused ion beam, ion beam sputtering, ion implantation, we will center on the synthesis and modification of nanostructures using subatomic particle radiations.

The laws of energy and momentum conservation describe that a moving particle will transfer part or full of its kinetic energy to target atoms when a collision occurs, corresponding to elastic or non-

View Article Online
DOI: 10.1039/D0TA06742C

elastic collision. Displacement threshold energy defines the minimum energy required by a target atom to be expelled from the atomic network through the knock-on collision of an energetic projectile. The ejected atom can either take an interstitial position in the lattice or leave the system. In either cases, once the target atoms are kicked out, vacancies are left at the original sites. Therefore, introduction of defects to the irradiated target is the most common objective from the bombardment of a particle radiation to a solid sample. In the selection of a proper particle beam for radiation of a specific target, it is of high significance to scrutinize and evaluate its particle type, particle energy, flux, and beam size.

3.2.1. Metals

Metal cations can be directly reduced by electrons, which lays the foundation for electron beam induced synthesis of metal nanostructures from appropriate precursors. The most common and accessible electron beam source is the electron microscope where a convergent electron beam functions as a 'light' source to visualize substances with sizes in the nanometer scale. Since the seminal demonstration of observing specimens in liquid, liquid-phase transmission/scanning electron microscope (TEM/SEM) has become a powerful toolkit that allows researchers to monitor the real-time nucleation, growth, ripening and transformation of NPs.[144, 145] *In-situ* synthesis of metal NPs within the TEM/SEM has also become a research frontier of increasing interest.[146-152] Fig. 6 illustrates common configurations of the liquid-phase electron microscopes. General synthetic scenarios include (a) colloidal NPs obtained from a homogeneous solution containing dissolved metal salts[153-155], (b) reduction of metal oxides or other oxidized compounds to metals[156-160], and (c) electron beam induced fragmentation of larger-sized metal particles into nano-sized particles.[161-163] Note worthily, thermal heating is inevitably accompanied with high-energy electron beam radiation due to the law of energy conservation.[13, 164] The temperature of irradiated sample could even be elevated to over 1000 °C.[165] The underlying driver to the synthesis of metal NPs thus

View Article Online
DOI: 10.1039/D0TA06742C

might be either or combination of electron reduction and thermal heating. Nevertheless, the limited size of specimen holder severely restrains the yield and the further application of as-obtained NPs. Such a strategy, to be more precise, is more applicable for the fundamental mechanistic understanding rather than for large-scale synthesis.

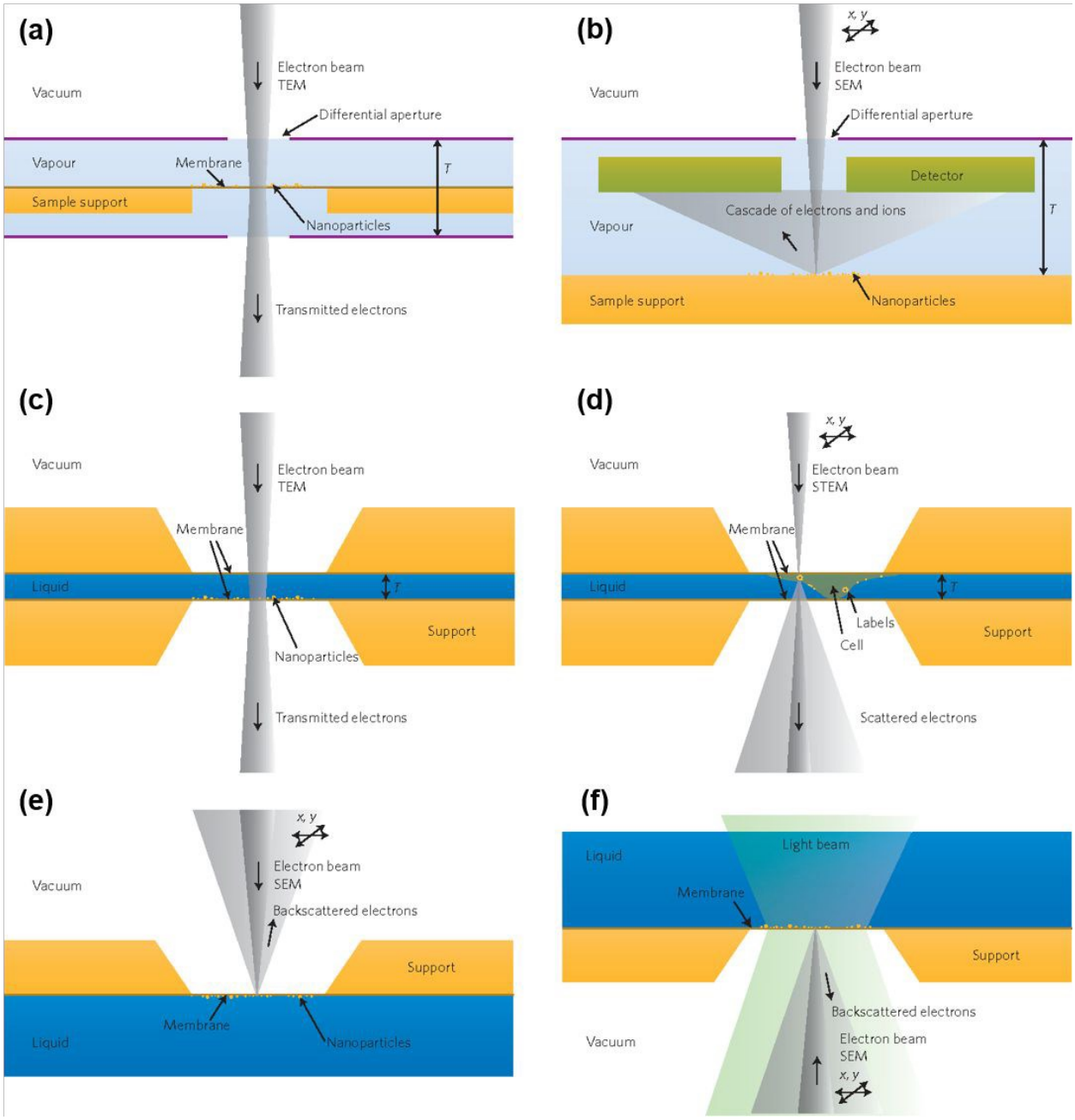

Fig. 6 Configurations for liquid-phase TEM/SEM. (a) TEM imaging with an open environmental chamber containing liquid and vapor. Differential apertures separate the microscope vacuum from

View Article Online
DOI: 10.1039/D0TA06742C

the higher pressure at the sample. (b) SEM imaging with an environmental chamber. The electron beam scans in *x* and *y* directions over the sample. (c) TEM imaging of NPs in a liquid fully enclosed between electron transparent windows. (d) STEM imaging in a fully enclosed liquid, used to image NP labels on whole biological cells. (e) SEM of a liquid sample under an electron transparent window. (f) Combination of SEM and light microscopy of a liquid sample above an electron transparent window. Adapted with permission.[150] Copyright 2011, Springer Nature.

Synthesis of metals outside of the TEM/SEM has also been well-documented. Lee and colleagues prepared PVP-stabilized Cu NPs in a solution of $CuSO_4$ dissolved in EG-IPA by electron beam radiation.[166] By controlling the beam energy, beam current and absorbed dose, the particle size of Cu NPs is fine-tuned. More specifically, higher beam energy and beam current result in smaller particles, while higher radiation dose leads to larger particles. The effect of PVA concentration and pH on the preparation of Cu NPs was systematically studied by Zhou and colleagues, revealing that the APS of Cu NPs, within a certain rage, decreases with increasing PVA concentration.[167] Colloidal Ag NPs stabilized by tannic acid and PVA were also prepared from an aqueous $AgNO_3$ solution by electron beam radiation.[168] This study found that high dose rate is required to obtain a good yield of Ag NPs. To compare the efficacy of electron beam and γ-ray in the radiolytic synthesis, Nguyen and co-workers synthesized chitosan-stabilized Au NPs by exposing an aqueous $HAuCl_4$ solution to electron beam and γ-ray radiations. At the same doses, Au NPs prepared by electron beam are significantly smaller than those by γ-rays. In another study by Seino and co-workers, the researchers prepared supported Au NPs in the presence of γ-Fe_2O_3 by electron beam and γ-rays.[169] It is found that electron beam results in smaller Au NPs than γ-rays, which is also attributed to the dose rate effect. Same results were reported by Korolkov and colleagues who found that Au NPs prepared by an electron beam had smaller sizes than those by γ radiation.[170] However, the efficiency of electron beam-induced reduction is lower than that of γ radiation, thus necessitating longer radiation time for Au NP formation by electron beam. These studies

View Article Online
DOI: 10.1039/D0TA06742C

collectively indicate that the generation rate of reducing species in the course of radiation is critical for controlling the size of NPs.

3.2.2. Metal Compounds

Application of particle radiation to metal compounds is largely limited to the modification instead of the synthesis. For example, the effect of defect creation is especially prominent for the irradiation of 2D TMCs by particle beams.[171-173] Considering the high density of atoms in a substance and the nature of particles, the penetration depth is normally shallower than ionizing electromagnetic waves and the radiation-induced modification mainly impacts the surface layers of a solid.

Baeck and co-workers irradiated MnO_2 powder by a proton beam so as to create oxygen vacancies.[174] The radiation is done either with dry MnO_2 powder or a dispersion of MnO_2 in water, as shown in Fig. 7a. MnO_2 irradiated in water is found to have more oxygen vacancies than that in dry powder. The authors reasoned that highly reactive radicals such as $O_2^{\bullet}$ and $OH^{\bullet}$ stemming from the radiolysis of water efficiently boost the cleavage of Mn–O bonds, indicating the important role of the medium in which the target exists. Using high-energy Ga^+ ion beam, Drndić and co-workers irradiated MoS_2 single layer with different ion doses.[175] The authors observed that angstrom-size vacancy defects are generated. These vacancies come from both Mo and S atoms that have been kicked out, and their sizes increase with high ion doses, as discerned in Fig. 7b. Similar observation is reported by Novoselov and colleagues who employed high-angle annular dark field (HAADF) imaging technique to directly discern the formation of vacancies when *in-situ* irradiating single layer MoS_2 with electron beam inside the TEM.[176]

View Article Online
DOI: 10.1039/D0TA06742C

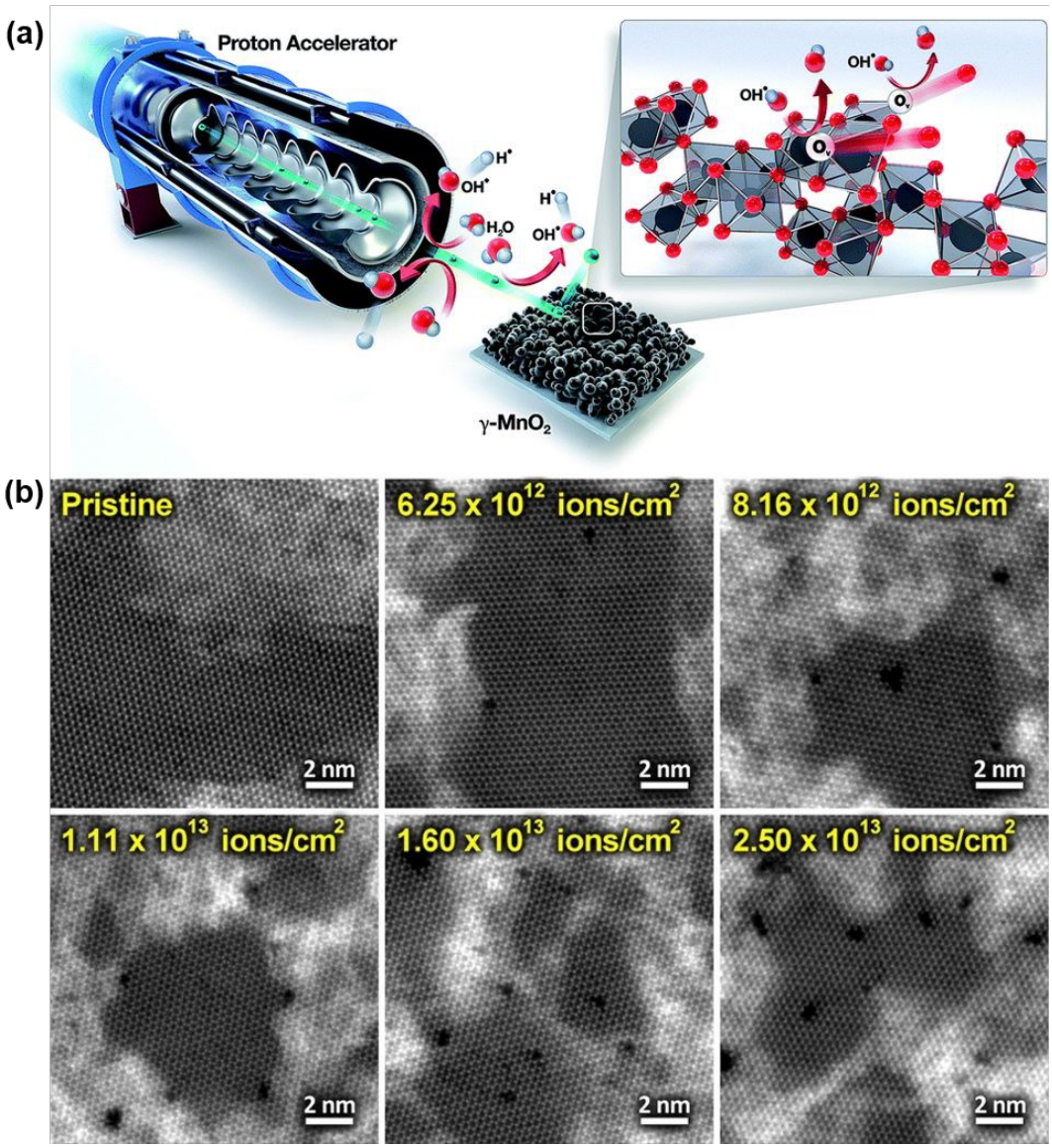

Fig. 7 (a) Schematic illustration of the preparation of oxygen-deficient MnO_2 NPs by proton beam irradiation. Reproduced with permission.[174] Copyright 2019, The Royal Society of Chemistry. (b) Aberration corrected STEM images of pristine and Ga^+ ion irradiated single-layer MoS_2 with different ion doses. Reproduced with permission.[175] Copyright 2018, American Chemical Society.

Phase and morphology of metal compounds are also susceptible to particle radiation. Recently, Suenaga and colleagues provided the first *in-situ* STEM observation of phase transition of single layer MoS_2 induced by electron beam.[177] At elevated temperatures of 400–700 °C, electron beam is found indispensable for the conversion between the semiconducting 2H (trigonal prismatic D_{3h}) and the metallic 1T (octahedral O_h) MoS_2 phases. Later, theoretical density functional theory

View Article Online
DOI: 10.1039/D0TA06742C

calculations unravel that the phase transition is related to the charge redistribution in the monolayer owing to the electronic excitations coupled with beam-induced formation of vacancies and the accumulation of resulting mechanical strain.[178, 179] When irradiating a bulk WS_2 crystal by a proton beam, Polimeni and co-workers observed a variation of its surface morphology.[180] Fig. 8a shows an AFM image of bulk WS_2 after irradiation at a dose of 8×10^{16} protons cm^{-2}. Quasi round-shaped dots are clearly observed on the surface. With a dose eight times smaller, similar dots but much smaller in sizes are formed (Fig. 8b). A close-up of the dots reveals that they are in essence domes with various heights (Fig. 8c). Accordingly, a formation mechanism of the domes is proposed and illustrated in Fig. 8d. High-speed protons traverse the topmost layer and recombine as H_2 molecules at the interlayer gap between the first and second layers. The accumulation of H_2 molecules leads to the blistering of one-monolayer thick domes. The domes are found very stable and their sizes are strongly related to the radiation dose.

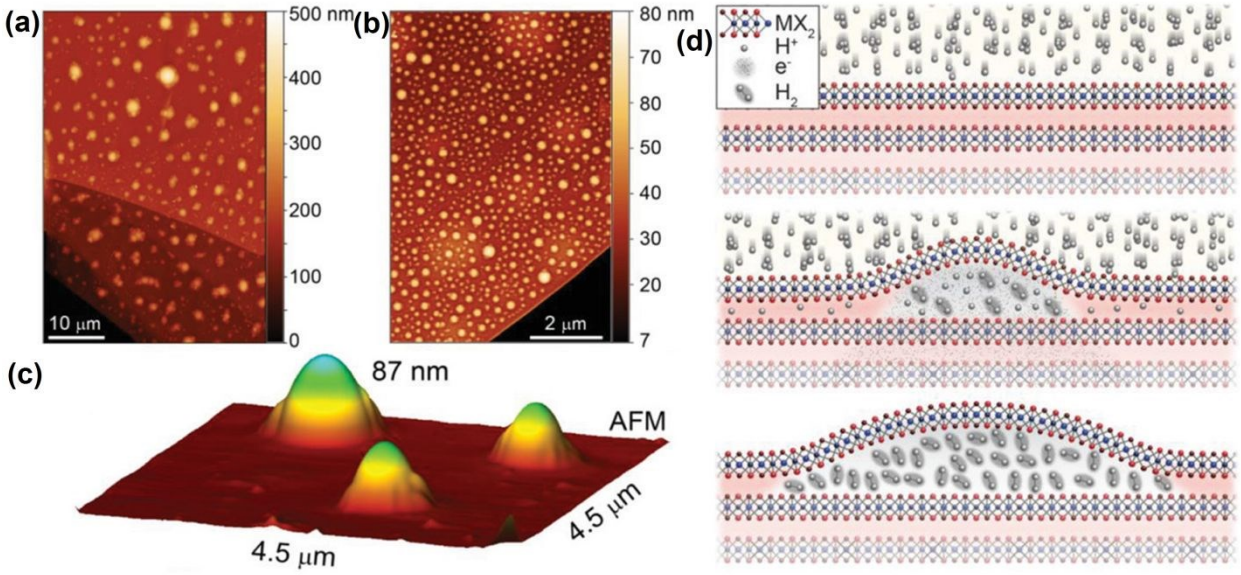

Fig. 8 Creation of light-emitting domes by proton irradiation. (a) AFM image of the bulk WS_2 after irradiation with proton dose of 8×10^{16} protons cm^{-2}. Round-shaped features on the sample surface form after proton irradiation. (b) AFM image of a proton irradiated bulk WS_2 flake with a dose eight times smaller than that in (a). (c) AFM image of a limited region of a sample treated same as that in (b) but on a different flake, where a smaller density of domes was fortuitously found. The maximal height reached by the domes is 87 nm. (d) Sketch of the process leading to the formation

View Article Online
DOI: 10.1039/D0TA06742C

of domes caused by the local blistering of atomically thin membrane materials. Adapted with permission.[180] Copyright 2019, Wiley-VCH.

3.2.3. Carbon

Investigation of nanostructured carbon materials by particle radiation can be traced back to the 1990s.[181-184] Since then, this field has stimulated a great deal of research trials. Apart from the intuitive perception that particle radiation introduces disorder to the irradiated substance, beneficial structural engineering with high precision by particle radiation is realizable to carbon systems. This would not be possible without the capability to converge the particle beam spot to a resolution of few nanometers or even few angstroms. Accordingly, perforation and bending[185], shrinking[186, 187], bridging[188], coalescence[189], cutting/sectioning[190], and welding[191] of the CNTs by electron beams have been experimentally implemented. Similar structural reconstructions have also been enabled by other ion beam radiations.[192-198] In the case of 2D graphene and GO, particle radiation creates defects, which has been directly visualized.[199] Reduction of GO in the way of removing oxygen functional groups has also been reported.[200, 201] Two excellent review articles specifically focusing on the radiation effects by particle beams on carbon nanostructures could be referred to for in-depth knowledge.[14, 202] Again, these particle radiations are mostly limited to the microscope and other *in-situ* instruments for fundamental research purposes.

Recently, Cigler and co-workers reported a readily scalable method to create structural defects through the irradiation of nanomaterials by light ions *in-situ* generated from a nuclear reaction.[203] As shown in Fig. 9, a neutron beam is shined to target NPs dispersed and encapsulated by a $^{10}B_2O_3$ glassy belt. The capture of neutrons by ^{10}B causes a nuclear reaction that generates an isotropic flux of α particles, $^{7}Li^{+}$ ions and γ-rays. The energetic light ions then kick out target atoms and create vacancies. Both diamond nanocrystals and cubic silicon carbide NPs are used as target NPs. It is found that fluorescent N vacancy color centers in the diamond and carbon antisite-vacancy

View Article Online
DOI: 10.1039/D0TA06742C

pairs in silicon carbide are uniformly and rapidly formed after the irradiation. Further testing in a nuclear reactor proves that this strategy is suitable for the large-scale mass production of defective NPs.

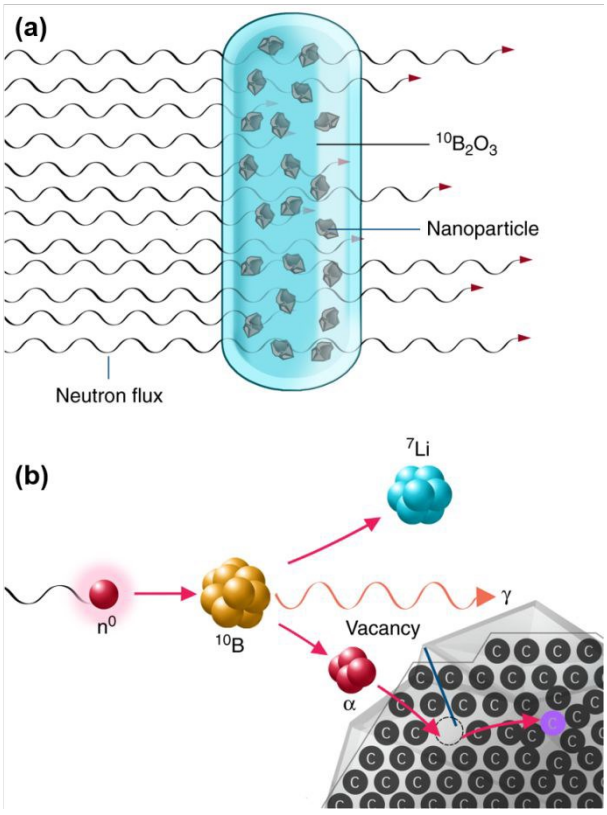

Fig. 9 Schematic illustration of the defect creation by bombardment of *in-situ* generated energetic ions to pre-existing NPs. (a) A container containing target NPs encapsulated by a glassy melt of $^{10}B_2O_3$ irradiated by a neutron flux. (b) Principle of α particles and $^7Li^+$ ions produced from the nuclear reaction between ^{10}B and captured neutrons entering a nanodiamond particle and creating vacancies inside. Reproduced with permission.[203] Copyright 2018, Springer Nature.

4. Non-Ionizing Radiation

4.1. UV Irradiation

The broadly accepted wavelength of UV resides in the range of 10–400 nm, corresponding to the photon energy of 3–120 eV. It can be further subdivided into near, middle, far, and extreme UV following the photon energy from low to high. Note that there is no clear boundary between

View Article Online
DOI: 10.1039/D0TA06742C

ionizing and non-ionizing radiations in terms of the photon energy. The far and extreme UV light could also be considered as ionizing radiation because the single photon energy is higher than the atomic ionization energy. Furthermore, alternative to the ionization radiation in which a single photon ionizes a large amount of atoms, collective behavior of multiple low-energy photons can also lead to the ionization with the release of excited electrons. Water ionization coupled with the generation of solvated electrons by UV is one of such examples. The vapor ionization energy threshold is around 12.6 eV and the band-gap energy of liquid water at 300 K is ~7–8 eV.[204-206] Even so, photoionization of water with the stroboscopic detection of nascent solvated electrons has been discovered by UV with photon energies as low as 3–5 eV.[207] Valuable reports can be referred to for further understanding of the photophysics of water.[208, 209]

In the electronic band structure of solids, the band gap normally refers to the energy difference between the top of the valence band and the bottom of the conduction band. Electrons excited from the valence band to the conduction band, also termed as hot electrons, can then move freely within the solid. Meanwhile, holes are created in the valence band as a result of the electron excitation. The band gaps of semiconductors, in all cases, are at the magnitude of few eVs. Therefore, hot electrons and holes can be facilely generated when irradiating semiconductors by the UV light. With the incorporation of a proper semiconductor as the photoinitiator, conduction band electrons and valence band holes can serve as *in-situ* reductants and oxidants, respectively.

Pulse laser ablation (PLA, Fig. 10a), especially liquid, is another mechanism for the synthesis and modification of materials using UV light. As a well-studied technique, PLA is often regarded as a physical top-down method instead of the aforementioned chemical one. Owing to the high intensity or photon flux, the irradiated bulk material is heated up by absorbing the photon energy, which then evaporates or sublimates at relatively low flux, or transforms to a plasma (a gas mixture of ions and electrons) at high flux. Photothermal effect due to the photon-matter interaction

View Article Online
DOI: 10.1039/D0TA06742C

mechanically ablates small particles from the raw material. In a liquid phase, the detached particles condensate to form a stable colloid that are readily available for anchoring to supporting materials. Further processing of the colloids by laser leads to laser fragmentation (PLF, Fig. 10b) or melting (PLM, Fig. 10c), in which the suspended particles are further fragmented to smaller sizes or melted to merge into larger sizes, respectively. Not limited to UV light, the laser source spans a wide range of wavelength to visible and IR lights, which will be discussed in the following sections as well. Several comprehensive reviews covering various aspects of the laser-assisted synthesis and processing of colloids are also available.[10, 12, 15, 210-214] It has been summarized that the target material properties (type, composition, shape), process parameters (time and post-treatment), liquid properties (solvent, precursor concentration, liquid height, additive, flow, viscosity, temperature, and pressure), and laser parameters (wavelength, pulse duration, pulse energy, fluence, spot size, and pulse repetition rate) are useful knobs for the on-demand synthesis and modification of various colloidal nanostructures. Laser can give rise to radiation effects induced by both single photon and multiple photons. Therefore, instead of repeating these details, we will mostly focus on new discoveries in the past 3 years.

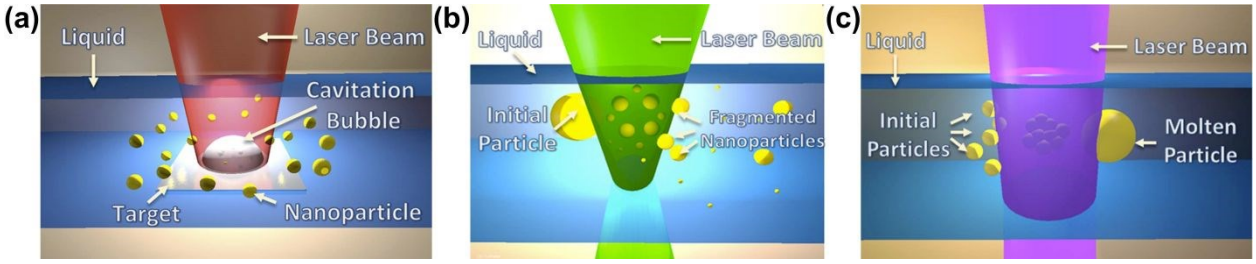

Fig. 10 Schematic illustrations of PLA (a), PLF (b) and PLM (c). A laser beam hits a target material, leading to the formation of cavitation bubble containing ablated particles that are spread into the liquid after the burst of the bubble (a). Initial large-sized particles in a colloid or suspension are fragmented by a laser beam into NPs (b). Initial small-sized particles are melted into a large-sized particles by a laser beam (c). Adapted with permission.[12] Copyright 2017, American Chemical Society.

View Article Online
DOI: 10.1039/D0TA06742C

4.1.1. Metals

Water photolysis resembles its radiolysis. Both processes generate solvated electrons and free radicals, but at distinctive reaction rates. Photoreduction of metal cations in an aqueous solution by UV irradiation for the preparation of metal nanostructures can be traced back to the last century.[215] However, the detailed mechanism and photolytic products of water photolysis still await further understanding. Prior to this, consensus has been reached that it is key to control the synthetic parameters during the nucleation and growth processes. Temperature is known as a critical kinetic parameter for downsizing to atomic scale.[216, 217] On that account, Wu and co-workers reported the UV-assisted synthesis of Pt single atoms by significantly decreasing the temperature to −25 °C.[218] Fig. 11 schematically outlines the synthetic processes of Pt single atoms by UV irradiation at room temperature and at iced temperature, respectively. Compared to the conventional photoreduction of H_2PtCl_6 in an aqueous solution, in which Pt atoms easily aggregate into NPs, the photoreduction conducted in an iced solution substantially mitigates the nucleation of Pt atoms, leaving the individual Pt atom as it is. Same strategy was also applied to the synthesis Pt single atomic catalyst at an ultralow temperature of −60 °C under the irradiation of UV light.[219] Surprisingly, Wang and co-workers fabricated Pt single atoms by irradiating solid state nitrogen-doped porous carbon pre-adsorbed with $PtCl_6^{2-}$ ions.[220] The authors suggested that $PtCl_6^{2-}$ ions are directly reduced by UV light but did not provide solid experimental evidence on this statement.

View Article Online
DOI: 10.1039/D0TA06742C

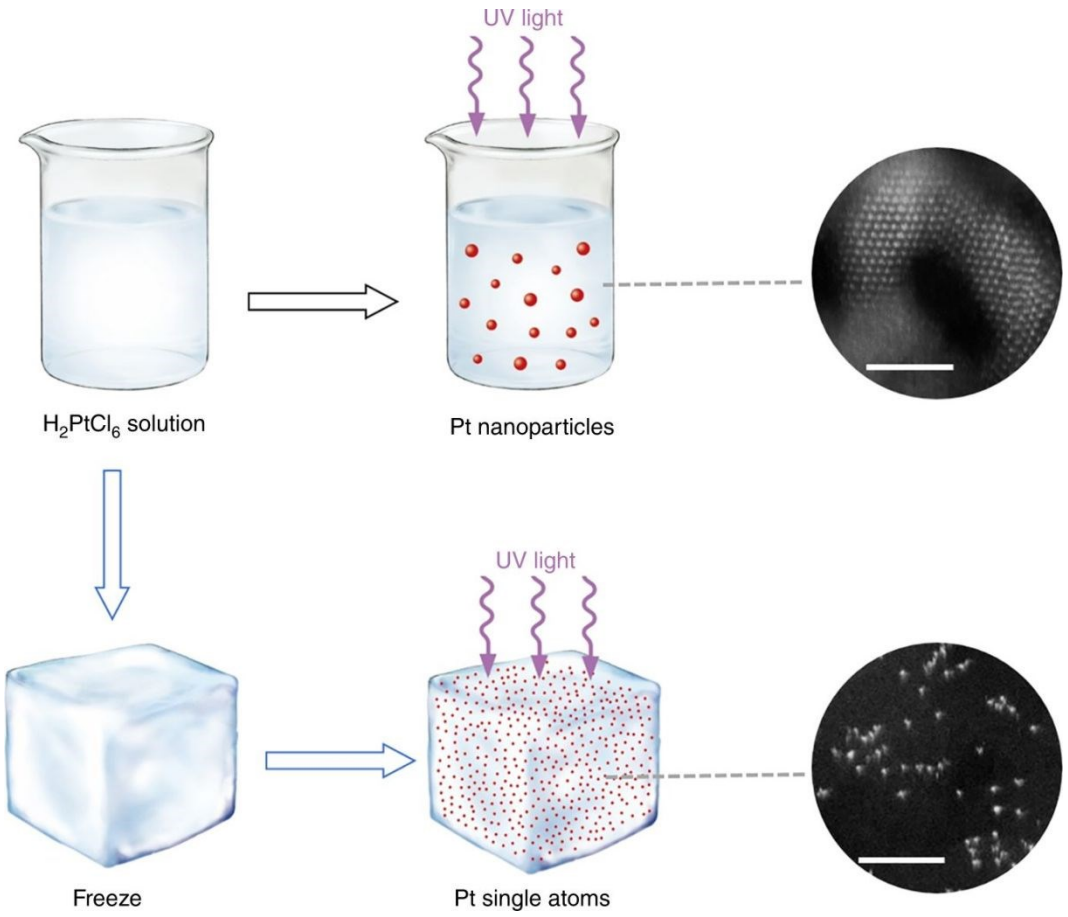

Fig. 11 Schematic illustration of the iced-photochemical synthesis. In the photochemical reduction of H_2PtCl_6 aqueous solution, Pt NPs are formed by the nucleation and agglomeration of Pt atoms (top row). Conversely, in the bottom row, we froze the H_2PtCl_6 solution prior to UV irradiation and obtained Pt single atoms dispersed in ice. The ice lattice naturally confined the ions/atoms and prevented their nucleation. (Scale bar, 2 nm) Reproduced with permission.[218] Copyright 2017, Springer Nature.

Other than water, there are also other photoactive materials that may function as the initiator of photoreduction by UV. Owing to the moderate band gaps, semiconducting materials are known as efficient photoinitiators. The hot electrons generated in semiconductors can reduce metal cations to atoms that are subsequently deposited on specific surface sites, leading to the formation of semiconductor–metal heterostructures.[221-223] Zheng and co-workers reported the preparation of atomically dispersed Pd supported on ultrathin TiO_2 nanosheets in EG solvent by UV treatment.[224] Fig. 12a illustrates the scheme of the UV-induced synthesis of Pd_1/TiO_2. Fourier-transformed

View Article Online
DOI: 10.1039/D0TA06742C

extended X-ray absorption fine structure (FT-EXAFS) spectra (Fig. 12b) shows that Pd atoms in Pd_1/TiO_2 are only bounded to surrounding oxygen atoms and no Pd–Pd metal bonds are formed, in sharp contrast to the Pd foil. HAADF-STEM image in Fig. 12c also verifies the formation of atomically dispersed Pd on TiO_2. Mechanistic study reveals that TiO_2 generates electron–hole pairs upon UV irradiation. Electrons reduce Ti^{4+} to Ti^{3+}, whereas holes generate EG radicals ($-OCH_2^{\bullet}CHOH$). Such radicals ultimately lead to the gradual stripping of Cl^- as HCl from $PdCl_4^{2-}$ and the bonding of remaining Pd atoms to oxygen atoms of TiO_2. Control experiments also demonstrate that EG radicals are vital for the formation of atomic Pd on TiO_2 instead of Pd NPs. In another study by Kamat and colleagues, the authors selectively anchored TiO_2 semiconductor and Ag NPs on GO using ethanol as the solvent.[225] Upon UV illumination, electrons are trapped by surface defect Ti^{4+} sites and holes are scavenged by ethanol. Once GO is added, the stored electrons are transferred to GO, leading to its reduction to rGO. Further addition of $AgNO_3$ induces the electron transfer from rGO to Ag^+ and the formation of Ag atoms, which eventually nucleate and grow as NPs that are anchored on rGO. The anchoring sites of Ag NPs are found different from the location of TiO_2, indicating the stepwise electron transfer process. Similar multicomponent composite is also reported by Shi and colleagues who deposit a series of noble metal NPs on graphene/ZnO support.[226]

View Article Online
DOI: 10.1039/D0TA06742C

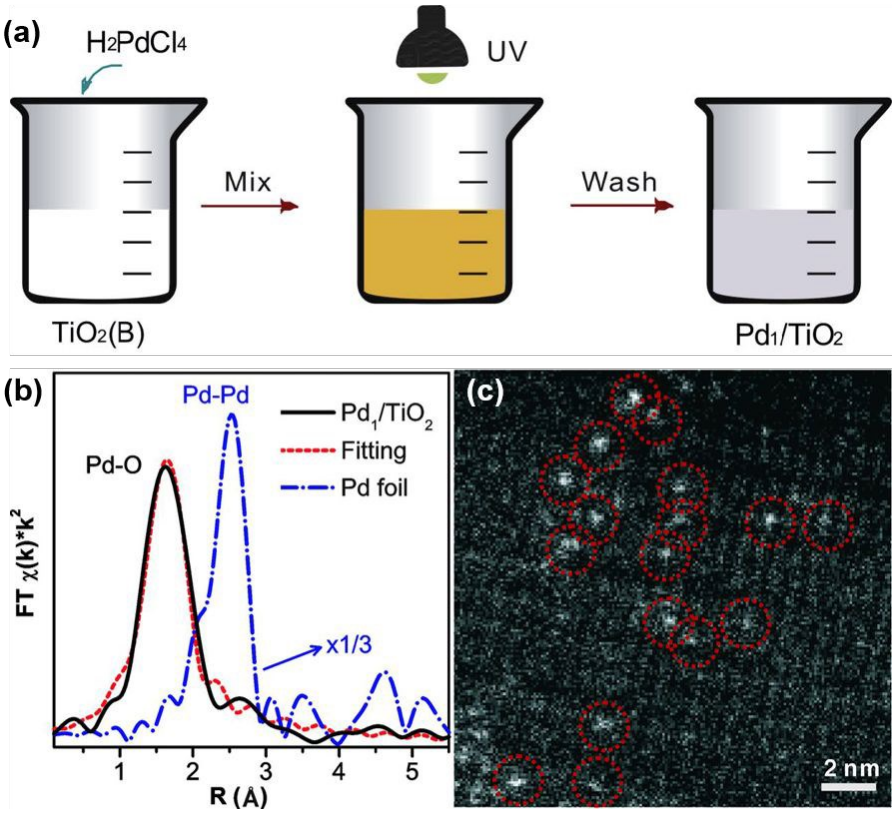

Fig. 12 (a) Schematic illustration of the photochemical synthesis of Pd_1/TiO_2. H_2PdCl_4 was introduced into water dispersion of TiO_2 to allow the adsorption of Pd species. The mixture was then irradiated by xenon lamp with low-density UV light for 10 min to obtain Pd_1/TiO_2. (b) FT-EXAFS spectra of Pd_1/TiO_2 and bulk Pd foil at the Pd K-edge, showing the adjacent atoms around Pd atoms. (c) High-resolution HAADF STEM image of Pd_1/TiO_2. The sample was calcined in air at 350 °C for better contrast. Adapted with permission.[224] Copyright 2016, American Association for the Advancement of Science.

To control the photodeposition process, Tossi and colleagues conducted a parametric study of the effect of UV light intensity, scavenger concentration, presence of H_2SO_4 acid, and precursor concentration on the size and distribution of Pt NPs on TiO_2.[227] It is found that low light intensity, low scavenger content, low precursor concentration, addition of H_2SO_4, and acidic pH are preferred to receive small and densely packed Pt NPs. Waclawik and co-workers investigated the rate of solid–liquid interfacial electron transfer in order to control the deposition of Au NPs on large ZnO NPs.[228] The authors discovered that solvent with low permittivity has higher rates of interfacial electron transfer than solvent mixture with high permittivity. High electron transfer rate empowers

View Article Online
DOI: 10.1039/D0TA06742C

the photoreduction of $AuCl_2^-$ ions at ZnO surface in less than 5 s, resulting in the formation of small and distributed ~6 nm Au NPs on the ZnO host. The preferred deposition sites of Au NPs on ZnO are under-coordinated facet edges and corner sites that readily trap the hot electrons and possess high electron accumulation. This is supported by the observation that Au deposition on ZnO capped with strong binding ligand dodecanethiol is largely retarded, in good agreement with previous findings that show site selective deposition of metal NPs on ZnO.[229, 230] In addition, oxygen content in the solvent and the UV illumination time are identified as critical factors that strongly influence the photodeposition process. These studies jointly demonstrate the importance of controlling synthetic conditions in terms of UV light, semiconductor, scavenger, solvent and precursor for engineering the photodeposition of metal NPs.

Organic photoinitiators are also reported for the synthesis of metal NPs by UV irradiation. Advincula and co-workers used 1-[4-(2-hydroxyethoxy)phenyl]-2-hydroxy-2-methyl-1-propan-1-one (HMP) to produce ketyl radicals as reducing agents by UV treatment.[231] Both GO and metal cation (Ag, Au, Pd) reduction are accomplished in a short period of time, leading to the formation of metal NPs/rGO composite. Han and co-workers reported the use of polystyrene-block-poly(4-vinylpyridine) (PS-*b*-P4VP) for the fabrication of Ag NPs on PS-*b*-P4VP diblock copolymer film.[232] The nitrogen atoms in pyridine ring are responsible for the chelation of Ag^+ ions. Upon UV irradiation, the pyridine ring generates electron−hole pairs, in which the electrons rapidly reduce chelated Ag^+ ions to Ag atoms.

Furthermore, UV PLA is applicable to prepare metal NPs from microparticles or bulk metals. Induced by the UV photons, a localized hot region with high temperature is formed and leads to the decomposition of PdO to Pd, which gives a PdO/Pd heterojunctions with tunable mass ratio.[233] In addition to PLA, PLF of metal NPs enables the preparation of smaller ultrafine NPs with high dispersity.[234]

View Article Online
DOI: 10.1039/D0TA06742C

4.1.2. Metal Compounds

Photothermal effect caused by UV light has also been demonstrated for the formation of metal oxides. Park and co-workers irradiated a film of metal alkoxides/hydroxides prepared by dissolving the nitrate/acetate precursors in 2-methoxyethanol solvent.[235] In an inert atmosphere, photothermal heating leads to the cleavage of alkoxy groups and facilitates the M–O–M network formation by condensation. Thus the sol–gel film is densified to an oxide film. UV radiation is also applicable to the modification of metal compounds. Driven by UV light, reversible doping and restoration of WS_2 were achieved by Eom and colleagues.[236] When irradiating in N_2, n-type doping is introduced to WS_2, whereas further UV illumination in O_2 restores the pristine features of WS_2.

Combining laser-induced fragmentation and photothermal effect on different components, Cao and co-workers synthesized ultrafine Co_3O_4 NPs on rGO by irradiating an aqueous suspension containing Co_3O_4 nanorods and GO.[237] Co_3O_4 nanorods go through the PLF process and split into ultrafine NPs. At the same time, localized high temperature and photogenerated electrons lead to the reduction of GO to rGO. Alternatively, PLA of a cobalt target in water by itself produces Co_3O_4 NPs without supporting materials or surfactant/ligand.[238] Ni-Fe layered double hydroxides were prepared by either PLA of an iron target in aqueous $Ni(NO_3)_2$ solution or PLA of a nickel target in aqueous $Fe(NO_3)_3$ solution.[239]

4.2. Visible Light Irradiation

The light perceivable to human eyes, or visible light, lies in a quite shallow wavelength range of 400–700 nm and a photon energy range of 1.8–3.1 eV. Similar to UV irradiation, multiphoton effect could also bring the ionization of solvent and the generation of active radicals and solvated electrons, which serve as *in-situ* reactants in the synthesis and/or modification. Among the visible

View Article Online
DOI: 10.1039/D0TA06742C

light-assisted synthesis and modification of nanomaterials, visible light laser constitutes the most powerful tool, which has been attempted for decades.[240-242]

4.2.1. Metals

Photoreduction by visible light laser is applicable for synthesis of metal NPs given the adequate selection of semiconducting materials.[243] Moussa and colleagues reported the visible light-induced co-reduction of metal cation and GO support for preparing metal NPs supported graphene.[244] GO could generate electron–hole pairs, of which the holes are scavenged by solvents and electrons serve as *in-situ* reductants for GO and metal cations. Furthermore, direct photoreduction has also been reported to prepare metal NPs. Tibbetts and co-workers compared the efficacy of 532 nm nanosecond (ns) laser pulses and 800 nm femtosecond (fs) laser pulses in the nucleation and growth of Au NPs without any additives or ligands.[245] By tuning the laser pulse energy, the authors received Au NPs with varied average sizes. (Fig. 13) It is observed that growth kinetics of Au NPs by ns laser pulses is less sensitive to pulse energy compared to that by fs laser pulses. Simulation studies unravel that the reduction of $AuCl_4^-$ to Au NPs by ns laser pulses proceeds via a photothermal autocatalytic mechanism coupled with surface plasmon resonance-enhanced fragmentation, distinct from the radical-mediated photoreduction by fs laser pulses. As a result, Au NPs prepared by ns laser pulses are equipped with small sizes of 5–7 nm and uniform distribution with a polydispersity index (PDI) of ~0.04 (Fig. 13). Lin and colleagues reported that carbon dots also generate electron−hole pairs by absorbing Xenon light.[246] Accordingly, Ru cations are reduced by the electrons to form NPs. Meanwhile, the possible thermal effect leads the evolution of pristine carbon dots into an encapsulation layer around the Ru NPs.

View Article Online
DOI: 10.1039/D0TA06742C

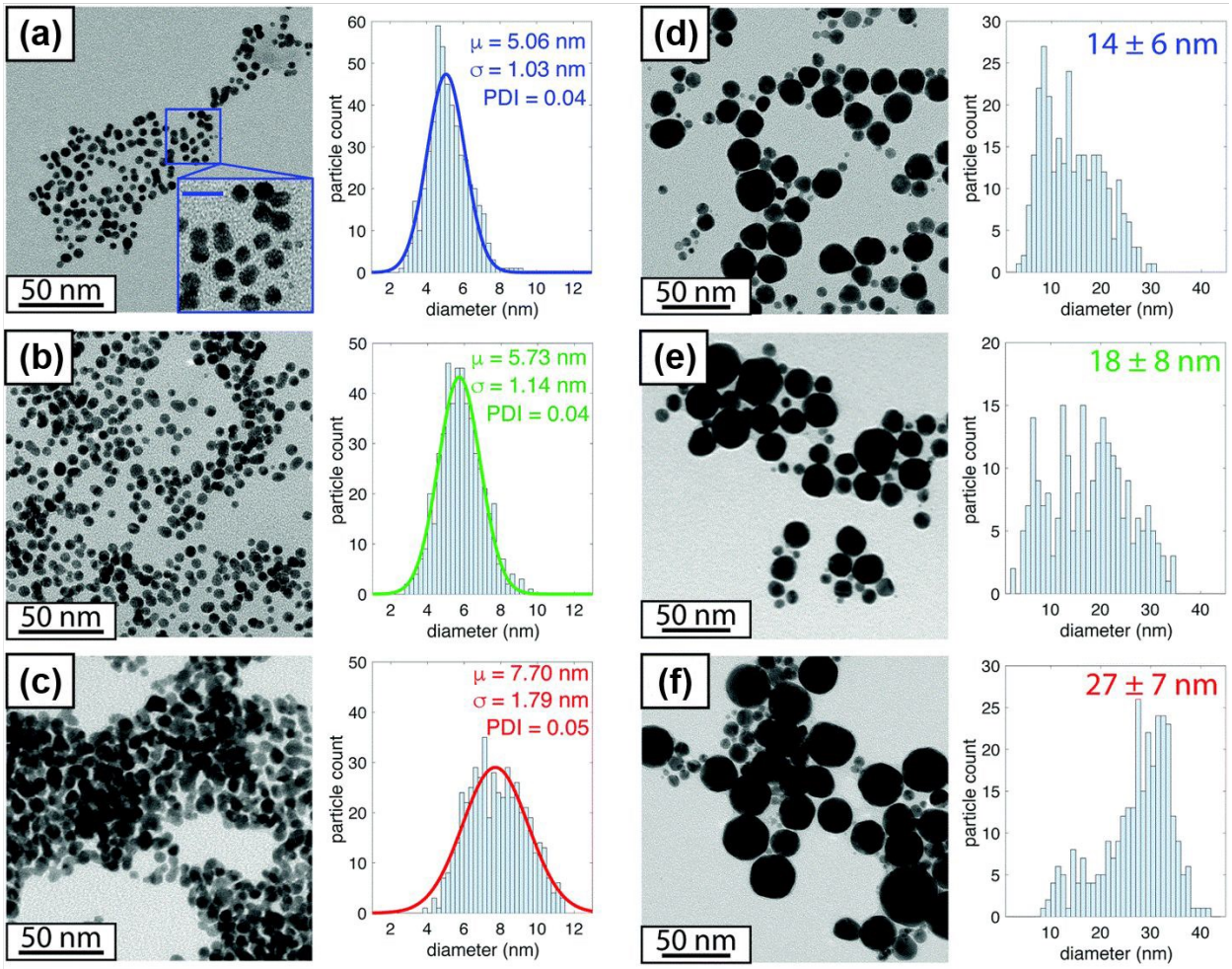

Fig. 13 TEM images and size distribution curves of Au NPs synthesized by 532 nm, 8 ns laser pulses with pulse energy of 100 mJ (a), 67 mJ (b) and 50 mJ (c), and by 800 nm, 30 fs laser pulses with pulse energy of 3.3 mJ (d), 3.0 mJ (e), and 2.7 mJ (f). The scale bar of the inset in (a) is 10 nm. Adapted with permission.[245] Copyright 2018, PCCP Owner Societies.

Laser-based techniques are used for the rapid synthesis of unconventional materials that are otherwise only reachable by complex, time-consuming and energy-intensive methods. Zheng and co-workers reported a laser-assisted strategy for the synthesis and structuring of immiscible RhAu alloys.[247] Fig. 14a illustrates the optical setup and ion accumulation. Upon laser illumination on the thermoplasmonic Au substrate, high thermal gradients are established and result in the formation of a microbubble trap (MBT). Under thermal gradients, convection affects the flow of metal cations and leads to the accumulation of cations in the vicinity of MBT. As a result, the cations are rapidly

View Article Online
DOI: 10.1039/D0TA06742C

reduced, giving an ultrahigh supersaturation within the limited zone. The nucleation and growth of RhAu alloys are thereby confined within a limited area. Through the stage translation and shutter on/off operations, the RhAu alloys can be patterned on the substrate. (Fig. 14b and 14c) TEM images in Fig. 14d and 14e confirm the formation of RhAu NPs with d lattice spacing of 0.235 nm. Advanced nanostructures are also obtainable by using pulsed lasers. Hampp and colleagues reported the PLA of a gold target in water glass solution.[248] The resulting Au NPs are found to be encapsulated by a thin SiO_2 layer.

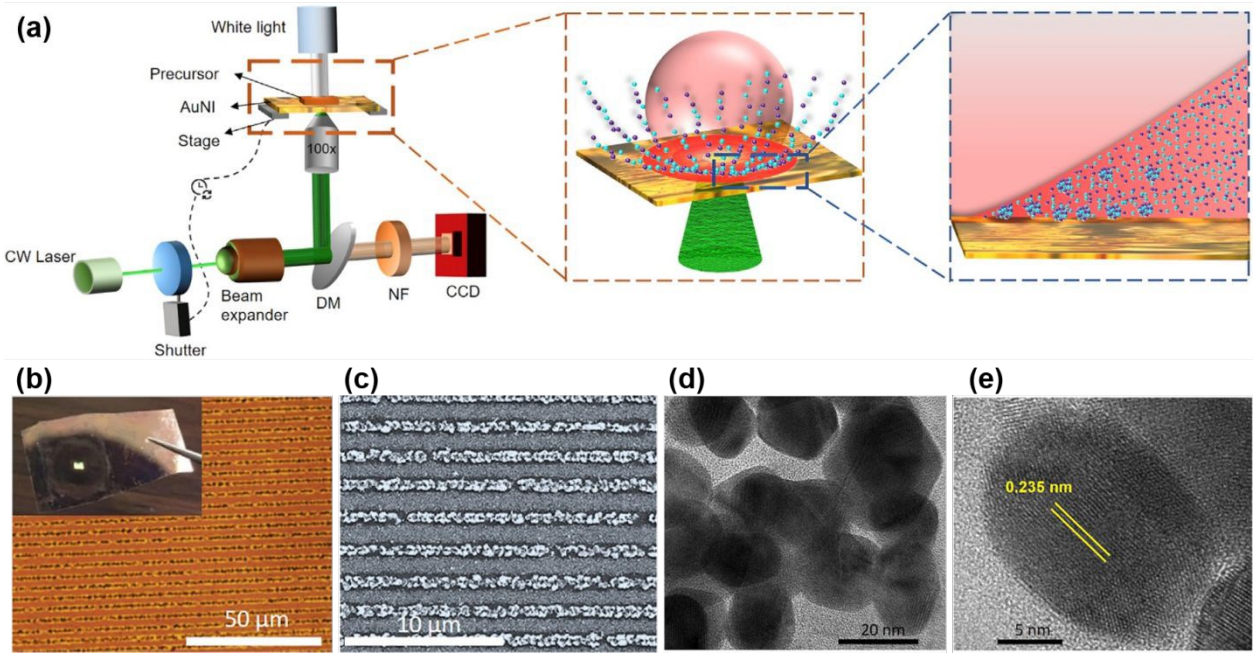

Fig. 14 (a) Schematic illustration of the optical setup and ion-accumulation. Laser-induced MBT leads to highly localized supersaturations of precursor ions in the vicinity of the MBT–substrate interface, enabling the simultaneous synthesis and patterning of RhAu alloys. (b) Optical image of the patterned RhAu alloys. The inset shows a completed sample of 2.25-mm^2 area. (c) SEM image of patterned alloys with 2-μm interline spacing. (d) TEM image of RhAu alloys. (e) High-resolution TEM image of RhAu alloys with lattice spacing indicated. Adapted with permission.[247] Copyright 2019, Elsevier Inc.

4.2.2. Metal Compounds

The potential of visible light laser in the modification of metal compounds has also been exploited. Using PLA technique, Saitow and co-workers reported the rapid synthesis of MoS_2 quantum dots (QDs) with a diameter of 4 nm in binary solvents of ethanol and water.[249] Micron-sized MoS_2

View Article Online
DOI: 10.1039/D0TA06742C

powder is dispersed in the mixed solvent and then irradiated by 532 nm nanosecond pulse laser for 20 min. The crystalline MoS_2 QDs consist of 3–5 layers and contain sulfur vacancy defects at an atomic concentration of 1%. The defect-rich MoS_2 QDs are found to present excellent electrocatalytic activity and blue luminescence property. In addition, laser induced defects have been reported to engineer other types of metal compounds. Carrier doping effect was revealed on large-scale WS_2 monolayers grown by van der Waals Epitaxy.[250] Defective cobalt oxide with Co^{2+} defects and oxygen vacancies was prepared by PLF of 8 nm oxide NPs.[251]

4.3. IR Irradiation

The photon energy of IR lies below the red light and its wavelength spans the range of 700 nm–1 mm, which can be subdivided into near, middle and far IR. IR frequency approximates the vibrational and rotational frequencies of molecular bonds. Thus, IR photons can be emitted or absorbed by molecules when changing the vibrational/rotational movements. The photon energy is insufficient to generate radicals and/or electrons, in stark contrast with UV and visible light. Utilization of IR radiation in material synthesis and modification is thus mostly limited to IR-based lasers.

4.3.1. Metals

IR laser-induced heating within the temporal scale of femtosecond or picosecond and the spatial limitation of irradiated spots opens a vast of opportunities in the synthesis of metal NPs.[252-257] As one of the examples, semiconductors can be activated by an IR laser to generate hot electrons that reduce metal ions to form NPs. In the presence of semiconducting MoS_2 nanosheets, Li and co-workers prepared metal–MoS_2 hybrids.[258] Fig. 15a illustrates that an IR laser induces the generation of electron–hole pairs. The electrons reduce the cations in the solution, leading to the deposition of

View Article Online
DOI: 10.1039/D0TA06742C

metal NPs onto MoS_2 nanosheets. As cases in point, ultrafine Ag (Fig. 15b and 15c) and Pt (Fig. 15d and 15e) NPs loaded on MoS_2 with high dispersity are prepared.

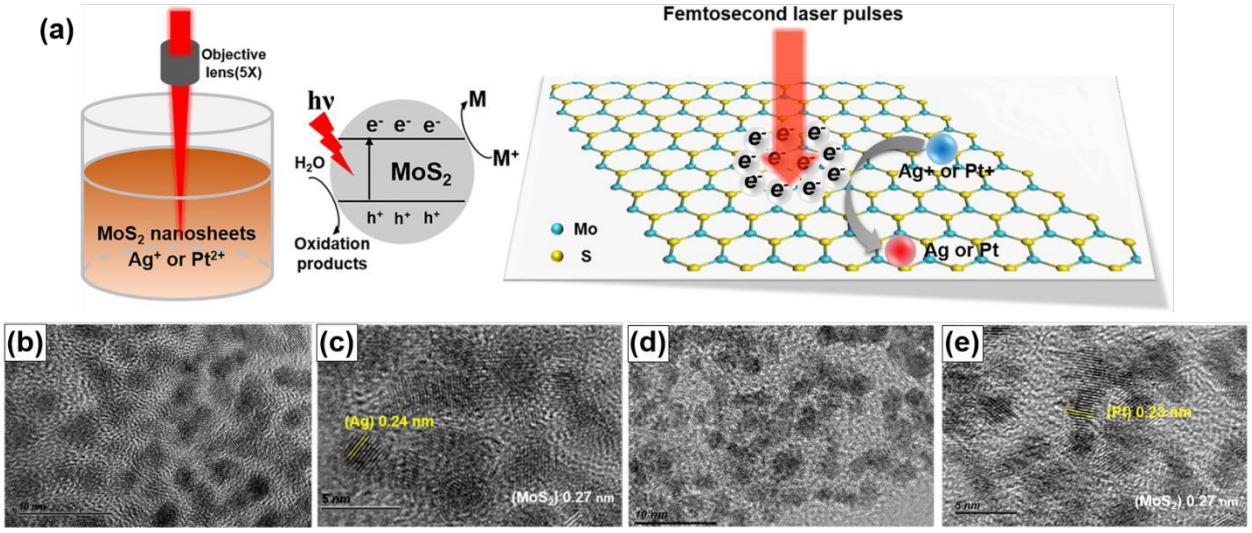

Fig. 15 (a) Schematic illustration of laser-induced decoration of MoS_2 with noble metal (Ag or Pt) NPs. TEM (b) and high-resolution TEM (c) images of the Ag−MoS_2 hybrids. TEM (d) and high-resolution TEM (e) images of the Pt−MoS_2 hybrids. Lattice spacings of MoS_2, Ag and Pt phases are indicated in (c) and (e). Adapted with permission.[258] Copyright 2018, American Chemical Society.

Advancing the traditional photoreduction of metal cations, Li and colleagues proposed the utilization of electrons from laser-induced plasma to prepare plasmonic nanostructures.[259] It is found that plasma-induced reduction has higher photon utilization efficiency in terms of colloidal NP yields than direct photoreduction of metal precursors. The NPs are also capable to self-assemble into shaped nanostructures directed by surface tension gradients between irradiated and unirradiated regions. Eychmgller and co-workers used a two-step strategy of PLA (1064 nm laser) followed by PLF (355 nm laser) to prepare noble metal aerogels.[260] The metal NPs are stabilized by electrostatic repulsion that arises from the inorganic ions in the aqueous solution.[261] By introducing a suited support, heterogeneous metal–support composites are also prepared by laser-based techniques.[262-265]

View Article Online
DOI: 10.1039/D0TA06742C

Mukherjee and colleagues combined PLA and galvanic replacement reaction (GRR) techniques to prepare ternary nanoalloys.[266] Cobalt pellet is rationally chosen as the target metal irradiated by a 1064 nm pulsed laser because of its lower Co/Co^{2+} redox potential (−0.28 V_{SHE}) than $PtCl_4^{2-}/Pt$ (0.76 V_{SHE}) and Cu^{+}/Cu (0.52 V_{SHE}). The GRR between ablated Co and two metal precursors (K_2PtCl_4 and CuCl) gives PtCuCo ternary nanoalloys. The PtCuCo alloy composition can be facilely tailored by varying the precursor concentration, solution pH, and ablation time. The target Co and metal precursor can also be replaced to obtain other ternary alloys. PLA method is also found to generate core–shell structures, such as the formation of metal@metal from a binary alloy target[267], metal@carbon by using an organic solvent[268-274] and from metal−organic frameworks (MOFs)[275], and metal@oxide in ethanol solvent[276].

4.3.2. Metal Compounds

IR PLA is capable of preparing metal compounds under desirable conditions. In 1 M KOH solution, PLA of Co target results in the formation of CoOOH nanosheets with abundant oxygen vacancies and relatively thin thickness.[277] IR PLA is also an effective tool for doping heteroatoms. Amans irradiated Gd_2O_3 target in an aqueous solution of $EuCl_3$ and attained Eu-doped Gd_2O_3.[278] IR PLF is proved as a valid strategy to embed small-sized NPs into a matrix with uniform distribution. Wang and co-workers fragmented a colloidal solution of originally 40 nm La-doped $BaSnO_3$ (LBSO) NPs into <10 nm NPs.[279] By mixing the newly-fragmented colloid solution with Mo-doped $BiVO_4$ (MBVO) precursor solution while keeping other preparation conditions unchanged, the authors managed to obtain MBVO film embedded with uniform LBSO nanocrystals.

High temperature and fast quenching created by laser favor the formation of compounds that are normally attainable by thermal heating in the furnace. Deng and colleagues reported a general laser metallurgy strategy to synthesize transition metal carbides.[280] MOF layers are irradiated by an IR

View Article Online
DOI: 10.1039/D0TA06742C

laser in air. The absorbed photons generate a high local temperature reaching up to 2620 °C with a heating rate of 6×10^5 °C s^{-1} and a cooling rate of 10^5 °C s^{-1}. Metal ions are instantaneously reduced, carbonized to form carbide NPs and quenched to prevent agglomeration. (Fig. 16a) Single phase carbides with sizes in the range of 6–20 nm are successfully prepared by changing the initial MOF. (Fig. 16b) Cheng and co-workers prepared Pt nanoclusters supported on defective CeO_2 by irradiating cerous MOF containing Pt ions with nanosecond IR laser.[281] Compared to the Pt@CeO_2 prepared by traditional furnace calcination, the laser technique endows Pt@CeO_2 with more defective CeO_2 surface and stronger metal-support coupling. (Fig. 16c) Melting of MOFs by femtosecond laser pulses allows the conversion of interpenetrated 3D MOFs comprising flexible ligands into well-organized spheres with a metal oxide dendrite core and amorphous organic shell.[282] Laser sculpturing is also a firm method to prepare metal carbides through the thermal effect.[283] When exposed to an IR laser, the precursors absorb the IR photon energy, which then generates high temperatures (over 1700 °C) within millisecond timescale. Carbon sources are "explosively" vaporized and reacts with metal ions to form macroporous carbides (e.g., MoC_x, WC_x, and CoC_x). Analogous to the formation of metal@carbon core–shell structures, IR lasers can also lead to the formation of compound@carbon[284-287] and metal@compound[288] core–shell structures.

View Article Online
DOI: 10.1039/D0TA06742C

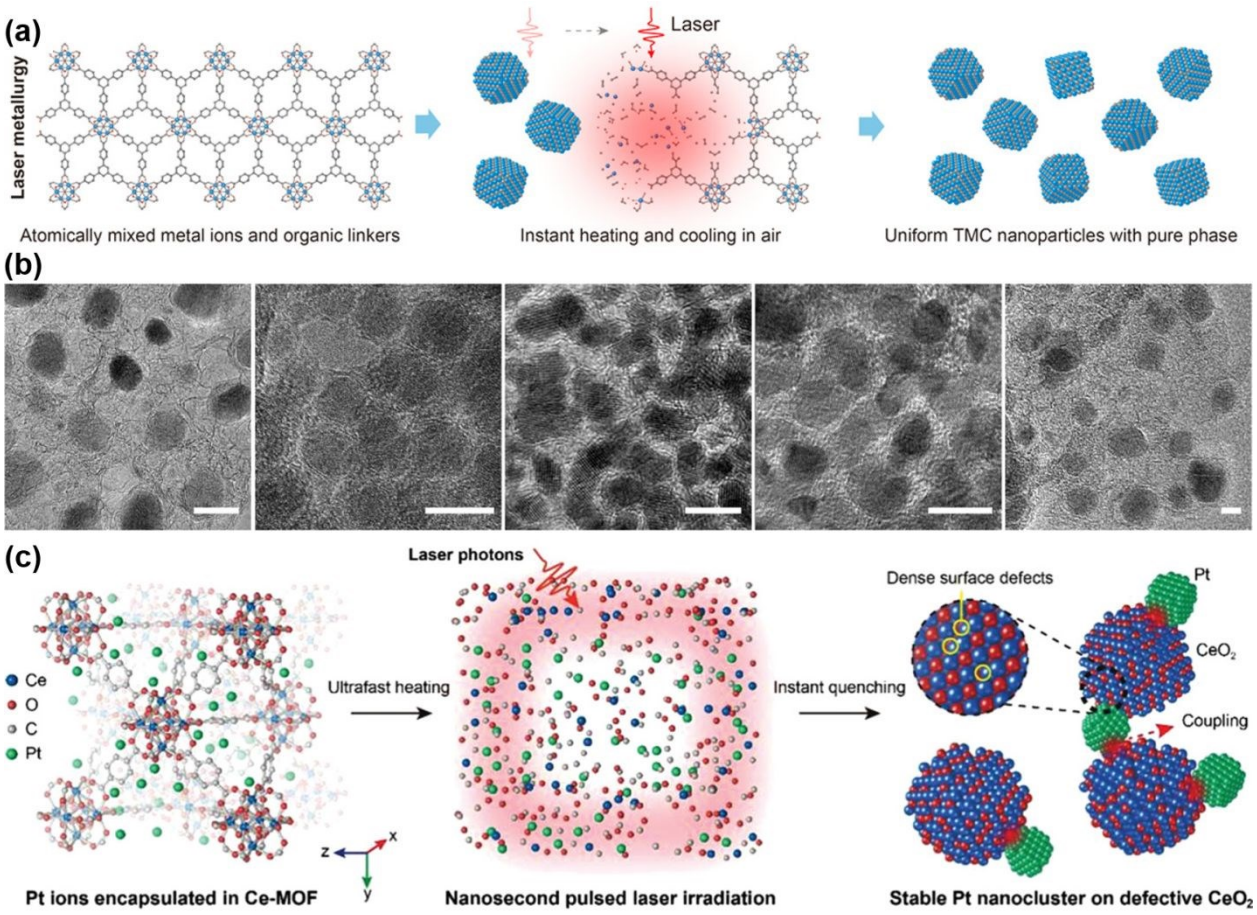

Fig. 16 (a) Laser metallurgy method for the synthesis of transition metal carbides. (b) TEM images of carbides. From left to right, ZrC, TiC, V_8C_7, α-MoC, and Cr_3C_2 NPs. Scale bar is 10 nm. Adapted with permission.[280] Copyright 2019, American Chemical Society. (c) Schematic illustration of the laser-induced formation of defective CeO_2 supported Pt nanoclusters. Reproduced with permission.[281] Copyright 2020, Wiley-VCH.

4.3.3. Carbon

Laser scribing has been proved as an efficient way to produce graphene membrane/patterns through the thermoreduction of GO[289-292] and carbonization of polyimide film[293-295]. A recent review article has especially focused on the laser-induced graphene.[296] The IR laser significantly elevates the local temperature on the irradiated substrate within in a short time period. GO is thus thermally reduced to graphene by removing the oxygen functional groups. Polyimide film is instantly carbonized into graphene. Moreover, one side of the graphene membrane is found to be

View Article Online
DOI: 10.1039/D0TA06742C

hydrophobic and the other hydrophilic, also known as Janus graphene. This strategy carries remarkable merits in the large-scale synthesis of flexible, patterned graphene membranes.

As an abundant source for carbon materials, heavy hydrocarbons have rarely been utilized as an affordable feedstock. Recently, Grossman and co-workers reported a laser treatment to heavy hydrocarbons, including tar, pitch and coal, for obtaining carbon materials ranging from amorphous to highly graphitic together with a broad distribution of electrical conductivity (Fig. 17a and 17b).[297] The authors demonstrated that finely tuning laser power, speed, and focus of the CO_2 laser source and carefully selecting the hydrocarbon feedstock allow the full control over the H:C ratio, sp^2 concentration, and degree of graphitic stacking order of the ablated products. The structural diversity of ablated products from laser-ablated heavy hydrocarbons is also revealed by the high-resolution TEM images in Fig. 17c, 17d and 17e. According to the fringes and the layer stacking, the graphitization degree of carbon products follows the order of coal (high), tar (medium) and pitch (low).

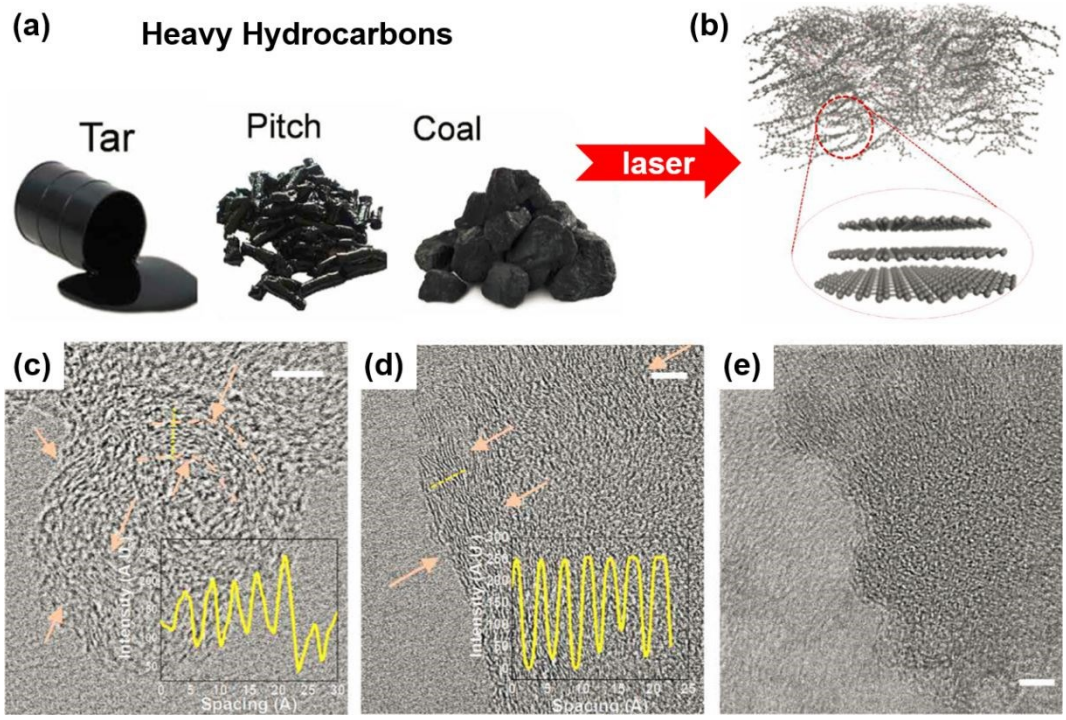

View Article Online
DOI: 10.1039/D0TA06742C

Fig. 17 (a) Heavy hydrocarbon materials: tar, pitch, and coal. (b) Laser-ablated stochastic graphitic system from heavy hydrocarbon. TEM images of laser-ablated steam cracked tar (c), low-volatile bituminous coal (d), and mesophase pitch (e). Arrows point to graphitic fringe stackings. All scale bars are 5 nm. Insets of (c) and (d) are profiles of highlighted lines. The average interlayer spacing of ablated tar is ~4.3 Å, and that of ablated coal is ~3.4 Å. Adapted with permission.[297] Copyright 2020, American Association for the Advancement of Science.

PLA and PLF have also been attempted for the preparation of carbon materials. Interestingly, Szymanski and co-workers found that an IR (1064 nm) laser pulse is more productive for carbon dots (CDots) than an UV (355 nm) laser pulse in the PLA of a graphite target due probably to the viscous solvent of polyethylene glycol 200.[298] PLA of graphite also generates CDots with smaller average sizes than that by PLF of an rGO suspension. In addition, pyrolysis of organic solvents driven by the laser-induced high temperature leads to the formation of CDots.[299] The solvent composition is tunable for doping of the CDots.

4.4. Microwave Irradiation

Microwave is an electromagnetic wave with a wavelength of 1 mm–1 m and a photon energy of 1.24 meV–1.24 μeV. Different from the electromagnetic spectrum with higher photon energy, the most relevant utilization of microwave for synthesis and modification of nanomaterials originates from the thermal heating mediated by microwave absorbing materials. Microwave radiation essentially is composed of oscillating electric and magnetic fields. A material absorbs the microwave through either the interaction with one of the two fields or both. Properties to describe such interactions with oscillating electric and magnetic fields are the bulk permittivity and permeability of a material, respectively. A material with high permittivity has its molecules randomly oriented with no internal electric field in total. When exposing this material to an external electric field, the rotational alignment of molecules is induced in a way that their electric dipoles are polarized, giving an internal electric field opposite to the external one. If the external field is oscillating at a high frequency, the molecules are thereby rotating at a high speed and the

View Article Online
DOI: 10.1039/D0TA06742C

temperature of these molecules is dramatically elevated. In this way, the absorbed microwave photons are dissipated as thermal energy. Energy dissipation in the form of magnetic rotation works in the same way for materials with high permeability. By far, various types of materials, including carbon, carbides, oxides, sulfides, phosphides, polymers, metals, and MOFs, have been reported as efficient microwave absorbers.[300] Most of the absorption is carried out in a liquid environment that limits the ramp rate and the ultimate temperature.[11] Renewed efforts have been made in optimizing the dielectric and magnetic properties of the absorbers to enhance the microwave–matter interaction and the energy conversion efficiency. The efficient energy conversion permits the rise of temperature to over 1000 °C in seconds or even quicker.

4.4.1. Metals and Compounds

Microwave-assisted synthetic method is often general and versatile to yield many types of materials. Either metal or compound NPs are attainable by following the same route but simply changing the precursor or the synthetic environment. We herein combine the discussions of metals and metal compounds in one subsection.

Transient thermal shock has been proved to synthesize well-dispersed and uniform-sized NPs by ultrafast heating and quenching.[301, 302] Hu and colleagues extended this tactics by utilizing microwave radiation.[303] As shown in Fig. 18a, by irradiating precursor loaded on rGO with microwave, a thermal shock is induced which leads to the formation of NPs homogeneously anchored on rGO. It is found that the temperature rises and stabilizes at around 1400 °C for subseconds during the microwave irradiation, which is followed by the rapid quenching (Fig. 18b). Using rGO with different amounts of defects (or oxygen functional groups), the authors discovered that optimal content of defects is necessary to enhance the photon absorption and maintain the thermal conduction (Fig. 18c). The photon absorption is further attributed to the polar oxygen functional groups that induce electric interaction with the electromagnetic field (Fig. 18d). Metal

View Article Online
DOI: 10.1039/D0TA06742C

(Ru, Pd and Ir) NPs are prepared using corresponding chloride precursors and CoS NPs are obtained using cobalt acetate and thiourea. Carbon black supported ultrafine Ru NPs are also synthesized by a similar microwave irradiation.[304] Differently, the amount of carbon black is suggested to be optimized due to the compromise between mass-driven microwave coupling and surface area-driven heat dissipation. When using a microwave absorber with moderate electronic conductivity, local Joule heating also becomes significant, which further elevates the temperature to ~2000 °C that otherwise is limited to below 900 °C by conventional microwave heating.[305] In addition, microwave-enabled fast heating with high peak temperature allows the synthesis of MOF-derived metal nanostructures.[306]

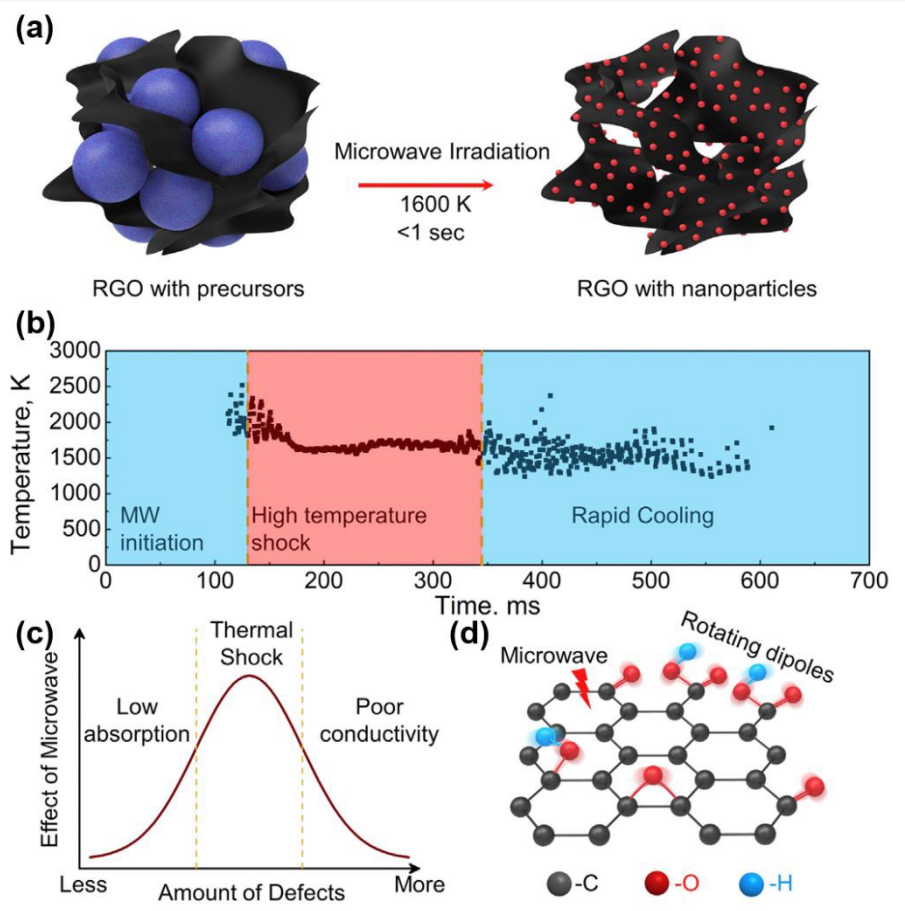

Fig. 18 (a) Schematic illustration of the thermal conversion from precursor/rGO (left) to NPs/rGO (right) by microwave irradiation. (b) Profile of average temperature captured during the microwave thermal shock. (c) The effect of defects on the thermal shock effect, showing that the thermal shock

View Article Online
DOI: 10.1039/D0TA06742C

effect only occurs when there is both good microwave absorption and good thermal conduction. (d) Depiction of the rotating dipole of the rGO functional groups during microwave irradiation. Reproduced with permission.[303] Copyright 2019, Elsevier Inc.

Microwave heating, like other types of radiations, has been reported for the preparation of single atomic metals. Despite that several methods have succeeded in the synthesis of single atomic metals anchors on carbon-based supports, pyrolysis of precursors at high temperatures remains the most prevailing one. Using the microwave heating, Duan and co-workers experimentally validated a general and efficient strategy to obtain graphene-supported single atomic metals.[307] GO is first functionalized with amino groups and then loaded with trace amount of metal precursors. After microwave irradiation of the freeze-dried precursors in argon for 5 seconds (3 seconds induction period and 2 seconds reaction period), the final products are received. The short time period prevents the possible agglomeration of metal atoms. Such a method is therefore regarded to be much more time-efficient than traditional pyrolysis in the electric furnace.

4.4.2. Carbon

Thermal heating by microwave is also viable for the synthesis and/or modification of carbon materials, especially in the case of thermal reduction/exfoliation from GO or graphite oxide to rGO and high-quality graphene.[308-312] However, the thermal process is not as straightforward as it seems to be. Chhowalla and co-workers reported a simple, rapid method to reduce GO in argon by 1- to 2-second microwave pulses.[313] The microwave-reduced GO is found to have higher quality than rGO prepared by conventional chemical reduction or high-temperature pyrolysis. More importantly, it is revealed that a moderate GO reduction step prior to the microwave radiation is prerequisite for the efficient absorption of microwave. The rapid heating then leads to the removal of oxygen functional groups and the restoration of sp^2-bonded carbon atoms. Later, Xu and colleagues found that direct microwave heating of graphite oxide in air takes 15–20 minutes to obtain exfoliated graphite oxide.[314] In contrast, in the presence of a small amount of graphite, it unexpectedly acts

View Article Online
DOI: 10.1039/D0TA06742C

as a catalyst to substantially accelerate the exfoliation process to just 2–3 seconds. It is deduced that the graphite powder with large π-domain is an efficient microwave absorber that delivers the photon energy to surrounding gas molecules. A plasma is thus generated to instantly reduce the graphite oxide.

5. Conclusions and Outlook

Synthesis and modification of nanomaterials lay the foundation of the unprecedented advancement of nanotechnology in various fields over the past years. Growing attention has been paid to developing preparation methods with high time efficiency, simplicity, and scalability as well as abidance by the concept of green chemistry. While Joule heating plays a dominating role in fueling the conventional synthesis and modification of inorganic nanomaterials, the low electric-to-thermal energy conversion efficiency due to the inevitable heat dissipation remains an issue to be tackled. The energy conversion efficiency is even lower when heating up to higher temperatures because of the larger temperature gradient relative to the environment, making it an energy-intensive and time-consuming process. Radiation in the forms of electromagnetic waves or energetic particle beams provides an alternative type of energy, which directly gives rise to atom/molecule ionization, electron transition, bond breaking, molecular transition, vibrational transition, and/or rotational transition to the irradiated substances. According to its energy, such radiations can be categorized as ionizing and non-ionizing. Ionizing radiations include γ-rays, X-rays, high-energy subatomic beams, and far UV, whereas non-ionizing consists of near UV, visible light, IR, microwave, and radio wave. Table 4 summarizes the applications of γ- and X-ray, particle beam, UV-visible-IR, and microwave radiations for the synthesis and modification of different types of inorganic materials together with their corresponding strengths and weaknesses. One of the shared advantages by these radiation techniques is the high versatility to various types of

View Article Online
DOI: 10.1039/D0TA06742C

materials. No conventional heating apparatus is required. Thereby, the issues related to uneven heat conduction facing traditional wet-chemical methods is effortlessly mitigated.

Table 4 Summary of the applications of different types of radiations and their corresponding strengths and weaknesses.

Radiation	Application	Strengths	Weaknesses
γ- and X-ray	• Synthesis of supported and unsupported metal NPs • Synthesis of oxides and sulfides • Surface engineering of carbon materials	▪ Ease of operation ▪ No reductants/oxidants ▪ Ambient conditions	○ Sedimentation ○ Poor structural control of NPs ○ Accessibility to radiation source ○ Removal of surfactant
Particle beam	• Synthesis of supported and unsupported metal NPs • Surface engineering of metal compounds and carbon materials	▪ Ease of operation ▪ No reductants/oxidants ▪ Ambient conditions ▪ *In-situ* observation using TEM	○ Low penetration ○ Poor structural control of NPs ○ Limited scalability ○ Accessibility to radiation source
UV, visible and IR	• Synthesis of metals and compounds in different sizes • Synthesis of carbon materials	▪ Time-saving and user-friendly ▪ Absence of surfactant ▪ Accessibility to radiation source	○ Poor size control ○ Presence of photoinitiator ○ Ambiguous mechanisms
Microwave	• Synthesis of metal and compound NPs • Synthesis of carbon materials	▪ Time-saving and user-friendly ▪ High thermal efficiency ▪ Absence of surfactant ▪ Accessibility to radiation source	○ Limited scalability ○ Presence of microwave absorbing materials

Among the radiation effects, atom/molecule ionization, electron transition, bond breaking lead to the production of active species, such as solvated electrons and free radicals, which serve as *in-situ* reductants or oxidants to replace foreign counterparts. On the other hand, molecular transition of photoinitiators results in the formation of electron–hole pairs, in which hot electrons and holes function as reductants and oxidants, respectively. Furthermore, vibrational and rotational transitions could cause ultrafast heating up to extreme temperatures from the atomic or molecular perspective. Note that in kinetic theory temperature corresponds to the motion of atoms and molecules. The high temperature pulse (rapid heating and quenching) results in the fast nucleation, growth and stabilization of NPs within the temporal scale of seconds or less. Advanced laser technology even strengthen the capability of UV, visible light and IR radiations. Laser-mediated photothermal effect and plasma generation can bring both chemical and physical reactions to the sample. Therefore, radiation-induced synthesis and modification of nanomaterials can avoid the

View Article Online
DOI: 10.1039/D0TA06742C

excessive usage of reductants/oxidants, shorten the reaction time, and reduce the energy consumption. These merits support all basic points required by the Green Chemistry.

Despite these remarkable promises, radiation technology still faces challenges prior to its widespread implementation in material synthesis and modification. Ionizing radiation sources are rare and not as easily accessible as traditional heating devices in every laboratory. Potential hazard to creatures exposed to such radiations keeps researchers alert and reluctant to exploit them. As a matter of fact, it is not quite the case as long as users strictly follow the standard protocols under the guidance of professionals. Therefore, more dissemination of the ionizing radiation in the future is called for the wide-spread promotion of this user-friendly technology. Non-ionizing radiations can be provided by a lamp or a laser source that is commercially available. Thus, the access is easier and the operation is safer given that the proper personal protection is provided and the corresponding regulations are followed.

In terms of synthesis and modification assisted by ionizing radiations, control of the size and distribution of NPs is not as straightforward as the well-established wet-chemical colloidal method. At a specific dose rate, G values of active species are constant, meaning that the generation rate of metal atoms is always fixed in the course of radiation. The dose rate is determined by the source and not quite freely adjustable, which is different from the colloidal synthesis as one can add the reactants faster or slower at will. Radiolytic synthesis of metal NPs in an aqueous system often requires the presence of surfactants/ligands to regulate the nucleation and growth processes to obtain small-sized and uniformly-distributed NPs. Alternative solvents have been attempted, but their radiolysis is still not fully clear, making it hard to preset the radiation parameters. Supporting materials can be added to anchor the formed NPs on the surface. However, the liquid system needs to be irradiated in an isolated and closed chamber where mechanical stirring to the system is barely possible to apply. Spontaneous sedimentation of supports implies that the NPs will not be loaded

View Article Online
DOI: 10.1039/D0TA06742C

uniformly because the lower part of solution is populated with more supporting materials than the upper part. Operation in the radiation chamber also causes scalability issues. The synthesis and modification are largely conducted batch by batch and the total volume is limited by the inner space of the chamber. Since the metal precursor concentration is relatively low, the yield of NPs hardly reaches subgram scale. Considering these issues, future directions in the research of ionizing radiation can be committed to (1) size control of NPs within confined space by taking advantage of the high penetration of radiation, (2) attempts of non-water solvents and understanding of the radiolytic mechanism, and (3) design of a flow reactor with part of it placed inside the chamber and exposed to the radiation so that the stock solution can be mobile.

Non-ionizing radiations inclusive of near UV, visible light, IR and microwave interact with substances at the molecular level. In all cases, the photon energy is absorbed if not reflected. The absorbed photon energy excites the kinetic motion that heats up the substance, especially in the case of a laser radiation. In light of this, the non-ionizing radiations can induce photothermal and photochemical effects. When a substance is being heated up to an extreme temperature, a plasma can be formed. Electrons in the plasma may also lead to chemical reactions. Precise clarification of the mechanisms in the synthesis and modification is thereby difficult. Photoinduced electron–hole pairs are often trapped at specific sites of the semiconductor, leading to the site-selective anchoring of NPs on the surface, whereas ionizing radiation generates solvated electrons and free radicals homogeneously throughout the whole liquid phase. It is therefore challenging to prepare heterogeneous structures with the metal NPs uniformly loaded on the support by means of photochemical reduction. Laser-mediated techniques, including PLA, PLF and PLM, are known to efficiently produce NPs with clean surface. However, the productivity of NPs is relatively low and the on-demand control of NP size, composition and morphology is uneasy to accomplish. Microwave radiation leads to the generation of thermal shock wave. The transient rise and fall of

View Article Online
DOI: 10.1039/D0TA06742C

high temperature restrain the opportunity to tailor the size and dispersity of NPs. All the challenges notwithstanding, future research efforts can be dedicated to (1) site-selective deposition of metal NPs on semiconducting support to investigate metal–support interactions, (2) in situ monitoring of materials prepared by non-ionizing radiations to understand the underlying formation mechanism, and (3) streamlined synthesis of membrane materials and patterning of 2D materials by advanced laser technology.

There might be other potential challenges and arising problems concerning the application of all kinds of radiations in the green synthesis and modification of inorganic nanomaterials. With ever-increasing interest being triggered and extensive attempts being made, this technique thus holds great promises and is worth awaiting for further advancement in the coming future.

Acknowledgement

KG thanks the starting grant 20205013 of Shaoxing University. AB acknowledges support of the Dalton Nuclear Institute, the University of Manchester (Dalton Fellowship) and EPSRC grant EP/R042179/1. ZY thanks the financial support from University of Stavanger.

References

1. R. Paull, J. Wolfe, P. Hebert and M. Sinkula, *Nat. Biotechnol.*, 2003, **21**, 1144–1147.
2. S. C. Currall, E. B. King, N. Lane, J. Madera and S. Turner, *Nat. Nanotechnol.*, 2006, **1**, 153–155.
3. M. Nasilowski, B. Mahler, E. Lhuillier, S. Ithurria and B. Dubertret, *Chem. Rev.*, 2016, **116**, 10934–10982.
4. J. W. Liu, H. W. Liang and S. H. Yu, *Chem. Rev.*, 2012, **112**, 4770–4799.
5. Y. Wu, D. Wang and Y. Li, *Chem. Soc. Rev.*, 2014, **43**, 2112–2124.
6. N. T. Thanh, N. Maclean and S. Mahiddine, *Chem. Rev.*, 2014, **114**, 7610–7630.
7. L. Wu, A. Mendoza-Garcia, Q. Li and S. Sun, *Chem. Rev.*, 2016, **116**, 10473–10512.
8. I. Obodovskiy, *Radiation: Fundamentals, Applications, Risks, and Safety*, Elsevier, 1st edn., 2019.
9. H. Kudo, *Radiation Applications*, Springer Singapore, 1st edn., 2018.
10. H. Palneedi, J. H. Park, D. Maurya, M. Peddigari, G. T. Hwang, V. Annapureddy, J. W. Kim, J. J. Choi, B. D. Hahn, S. Priya, K. J. Lee and J. Ryu, *Adv. Mater.*, 2018, **30**, 1705148.
11. M. Tsuji, M. Hashimoto, Y. Nishizawa, M. Kubokawa and T. Tsuji, *Chem. Eur. J.*, 2005, **11**, 440–452.
12. D. Zhang, B. Gokce and S. Barcikowski, *Chem. Rev.*, 2017, **117**, 3990−4103.

View Article Online
DOI: 10.1039/D0TA06742C

13. I. G. Gonzalez-Martinez, A. Bachmatiuk, V. Bezugly, J. Kunstmann, T. Gemming, Z. Liu, G. Cuniberti and M. H. Rummeli, *Nanoscale*, 2016, **8**, 11340–11362.
14. A. V. Krasheninnikov and F. Banhart, *Nat. Mater.*, 2007, **6**, 723–733.
15. S. Barcikowski and G. Compagnini, *Phys. Chem. Chem. Phys.*, 2013, **15**, 3022–3026.
16. D. M. Clifford, C. E. Castano and J. V. Rojas, *Radiat. Phys. Chem.*, 2017, **132**, 52–64.
17. K. Čubová and V. Čuba, *Radiat. Phys. Chem.*, 2019, **158**, 153–164.
18. Z. Xu, L. Chen, B. Zhou, Y. Li, B. Li, J. Niu, M. Shan, Q. Guo, Z. Wang and X. Qian, *RSC Adv.*, 2013, **3**, 10579–10597.
19. I. Favier, D. Pla and M. Gomez, *Chem. Rev.*, 2020, **120**, 1146−1183.
20. S. Zhou, M. Zhao, T.-H. Yang and Y. Xia, *Mater. Today*, 2019, **22**, 108–131.
21. M. B. Gawande, A. Goswami, F. X. Felpin, T. Asefa, X. Huang, R. Silva, X. Zou, R. Zboril and R. S. Varma, *Chem. Rev.*, 2016, **116**, 3722–3811.
22. Y. T. Liao, N. V. Chi, N. Ishiguro, A. P. Young, C. K. Tsung and K. C. W. Wu, *Appl. Catal. B: Environ.*, 2020, **270**, 118805.
23. H. Konnerth, B. M. Matsagar, S. S. Chen, M. H. G. Prechtl, F. K. Shieh and K. C. W. Wu, *Coordin. Chem. Rev.*, 2020, **416**, 213319.
24. Y.-T. Liao, B. M. Matsagar and K. C. W. Wu, *ACS Sustainable Chem. Eng.*, 2018, **6**, 13628–13643.
25. E. Doustkhah, J. Lin, S. Rostamnia, C. Len, R. Luque, X. Luo, Y. Bando, K. C. Wu, J. Kim, Y. Yamauchi and Y. Ide, *Chem. Eur. J.*, 2019, **25**, 1614–1635.
26. C.-C. Chueh, C.-I. Chen, Y.-A. Su, H. Konnerth, Y.-J. Gu, C.-W. Kung and K. C. W. Wu, *J. Mater. Chem. A*, 2019, **7**, 17079–17095.
27. C. C. Lee, C. I. Chen, Y. T. Liao, K. C. Wu and C. C. Chueh, *Adv. Sci.*, 2019, **6**, 1801715.
28. J. Wang, Y. Xu, B. Ding, Z. Chang, X. Zhang, Y. Yamauchi and K. C. Wu, *Angew. Chem. Int. Ed.*, 2018, **57**, 2894–2898.
29. M. R. Benzigar, S. N. Talapaneni, S. Joseph, K. Ramadass, G. Singh, J. Scaranto, U. Ravon, K. Al-Bahily and A. Vinu, *Chem. Soc. Rev.*, 2018, **47**, 2680–2721.
30. X. Liu and L. Dai, *Nat. Rev. Mater.*, 2016, **1**, 16064.
31. A. Appleby and H. A. Schwarz, *J. Phys. Chem.*, 1969, **73**, 1937–1941.
32. S. Le Caër, *Water*, 2011, **3**, 235–253.
33. H. Fujita, M. Izawa and H. Yamazaki, *Nature*, 1962, **196**, 666−667.
34. A. Henglein, *Ber. Bunsenges. Phys. Chem.*, 1977, **81**, 556–561.
35. A. Henglein and R. Tausch-Treml, *J. Colloid Interface Sci.*, 1981, **80**, 84–93.
36. K. Kurihara, J. Kizling, P. Stenius and J. H. Fendler, *J. Am. Chem. Soc.*, 1983, **105**, 2574–2579.
37. J. L. Marignier, J. Belloni, M. O. Delcourt and J. P. Chevalier, *Nature*, 1985, **317**, 344−345.
38. Y. Zhu, Y. Qian, Y. Li, W. Wang, M. Zhang, Z. Chen and S. Tan, *Nanostruct. Mater.*, 1994, **4**, 915–918.
39. Y. Zhu, Y. Qian, M. Zhang, Z. Chen, B. Lu and G. Zhou, *Mater. Sci. Eng.: B*, 1994, **23**, 116–119.
40. B. Keita, L. Nadjo, C. de Cointet, J. Amblard and J. Belloni, *Chem. Phys. Lett.*, 1996, **249**, 297–303.
41. Y. Liu, Y. Qian, M. Zhang, Z. Chen and C. Wang, *Mater. Lett.*, 1996, **26**, 81–83.
42. T. Li, H. G. Park and S.-H. Choi, *Mater. Chem. Phys.*, 2007, **105**, 325–330.
43. M. Z. Kassaee, A. Akhavan, N. Sheikh and R. Beteshobabrud, *Radiat. Phys. Chem.*, 2008, **77**, 1074–1078.
44. S. P. Ramnani, J. Biswal and S. Sabharwal, *Radiat. Phys. Chem.*, 2007, **76**, 1290–1294.
45. S. Seino, T. Kinoshita, Y. Otome, T. Maki, T. Nakagawa, K. Okitsu, Y. Mizukoshi, T. Nakayama, T. Sekino, K. Niihara and T. A. Yamamoto, *Scr. Mater.*, 2004, **51**, 467–472.
46. M. R. Karim, K. T. Lim, C. J. Lee, M. T. I. Bhuiyan, H. J. Kim, L.-S. Park and M. S. Lee, *J. Polym. Sci. A: Polym. Chem.*, 2007, **45**, 5741–5747.
47. B. L. Gratiet, H. Remita, G. Picq and M. O. Delcourt, *J. Catal.*, 1996, **164**, 36–43.
48. W. T. Wu, L. Shi, Y. Wang, W. Pang and Q. Zhu, *Nanotechnology*, 2008, **19**, 125607.
49. K. Torigoe, H. Remita, P. Beaunier and J. Belloni, *Radiat. Phys. Chem.*, 2002, **64**, 215–222.

View Article Online
DOI: 10.1039/D0TA06742C

50. M. Treguer, C. de Cointet, H. Remita, J. Khatouri, M. Mostafavi, J. Amblard, J. Belloni and R. de Keyzer, *J. Phys. Chem. B*, 1998, **102**, 4310−4321.
51. Z. Zhang, T. M. Nenoff, J. Y. Huang, D. T. Berry and P. P. Provencio, *J. Phys. Chem. C*, 2009, **113**, 1155–1159.
52. F. a. Ksar, L. Ramos, B. Keita, L. Nadjo, P. Beaunier and H. Remita, *Chem. Mater.*, 2009, **21**, 3677−3683.
53. J. V. Rojas, M. C. Molina Higgins, M. Toro Gonzalez and C. E. Castano, *Appl. Surf. Sci.*, 2015, **357**, 2087–2093.
54. N. Misra, J. Biswal, A. Gupta, J. K. Sainis and S. Sabharwal, *Radiat. Phys. Chem.*, 2012, **81**, 195–200.
55. Q. Zhang, S. Ye, X. Chen, X. Song, L. Li and X. Huang, *Appl. Catal. B: Environ.*, 2017, **203**, 673–683.
56. K. Naghavi, E. Saion, K. Rezaee and W. M. M. Yunus, *Radiat. Phys. Chem.*, 2010, **79**, 1203–1208.
57. A. C. Dhayagude, A. Das, S. S. Joshi and S. Kapoor, *Colloids Surf. A*, 2018, **556**, 148–156.
58. X. Zhao, N. Li, M. Jing, Y. Zhang, W. Wang, L. Liu, Z. Xu, L. Liu, F. Li and N. Wu, *Electrochim. Acta*, 2019, **295**, 434–443.
59. J. Chen, F. Chen, Y. Wang, M. Wang, Q. Wu, X. Zhou and X. Ge, *RSC Adv.*, 2016, **6**, 55878–55883.
60. C. H. Zhu, Z. B. Hai, C. H. Cui, H. H. Li, J. F. Chen and S. H. Yu, *Small*, 2012, **8**, 930–936.
61. Z. I. Ali, O. A. Ghazy, G. Meligi, H. H. Saleh and M. Bekhit, *Adv. Polym. Technol.*, 2018, **37**, 365–375.
62. T. M. Nenoff, S. R. Ferriera, J. Huang and D. J. Hanson, *J. Nucl. Mater.*, 2013, **442**, 162–167.
63. A. Abedini, E. Saion, F. Larki, A. Zakaria, M. Noroozi and N. Soltani, *International Journal of Molecular Sciences*, 2012, **13**, 11941–11953.
64. A. Abedini, F. Larki, E. Saion, A. Zakaria and M. Z. Hussein, *Radiat. Phys. Chem.*, 2012, **81**, 1653–1658.
65. Z. Zhang, T. M. Nenoff, K. Leung, S. R. Ferreira, J. Y. Huang, D. T. Berry, P. P. Provencio and R. Stumpf, *J. Phys. Chem. C*, 2010, **114**, 14309–14318.
66. M. C. Molina Higgins, D. M. Clifford and J. V. Rojas, *Appl. Surf. Sci.*, 2018, **427**, 702–710.
67. C. R. Walker, K. Pushpavanam, D. G. Nair, T. Potta, C. Sutiyoso, V. D. Kodibagkar, S. Sapareto, J. Chang and K. Rege, *Langmuir*, 2013, **29**, 10166–10173.
68. V. I. Feldman, A. A. Zezin, S. S. Abramchuk and E. A. Zezina, *J. Phys. Chem. C*, 2013, **117**, 7286−7293.
69. J. V. Rojas and C. H. Castano, *Radiat. Phys. Chem.*, 2012, **81**, 16–21.
70. A. A. Melvin, V. S. Joshi, D. C. Poudyal, D. Khushalani and S. K. Haram, *ACS Appl. Mater. Interfaces*, 2015, **7**, 6590–6595.
71. K. M. Samant, V. S. Joshi, G. Sharma, S. Kapoor and S. K. Haram, *Electrochim. Acta*, 2011, **56**, 2081–2086.
72. S. W. Choi, S. H. Jung and S. S. Kim, *Journal of Hazardous Materials*, 2011, **193**, 243–248.
73. H.-J. Ahn, J.-S. Lee, H.-S. Kim, I.-T. Hwang, J.-H. Hong, J. Shin and C.-H. Jung, *J. Ind. Eng. Chem.*, 2018, **65**, 318–324.
74. Z. Zhang, X. Cui, W. Yuan, Q. Yang, H. Liu, H. Xu and H.-L. Jiang, *Inorg. Chem. Front.*, 2018, **5**, 29–38.
75. S. J. Wang, Y. W. Zhang, H. L. Ma, Q. L. Zhang, W. G. Xu, J. Peng, J. Q. Li, Z. Z. Yu and M. L. Zhai, *Carbon*, 2013, **55**, 245–252.
76. A. Abedini, M. Saraji, A. A. A. Bakar, P. Susthitha Menon and S. Shaari, *Plasmonics*, 2017, **13**, 771–778.
77. H. K, R. P. Joshi, S. D.V, V. N. Bhoraskar and S. D. Dhole, *Appl. Surf. Sci.*, 2016, **389**, 1050–1055.
78. K. Guo, L. J. Rowland, L. H. Isherwood, G. Glodan and A. Baidak, *J. Mater. Chem. A*, 2020, **8**, 714–723.
79. Q. Zhang, Y. Zhang, Z. Gao, H.-L. Ma, S. Wang, J. Peng, J. Li and M. Zhai, *J. Mater. Chem. C*, 2013, **1**, 321–328.
80. H.-Y. Park, D.-S. Yang, D. Bhattacharjya, M. Y. Song and J.-S. Yu, *Int. J. Hydrogen Energy*, 2014, **39**, 1688–1697.
81. T. Cele, M. Maaza and A. Gibaud, *MRS Adv.*, 2018, **3**, 2537–2557.
82. V. M. Rao, C. H. Castano, J. Rojas and A. J. Abdulghani, *Radiat. Phys. Chem.*, 2013, **89**, 51–56.

View Article Online
DOI: 10.1039/D0TA06742C

83. V. Hornebecq, M. Antonietti, T. Cardinal and M. Treguer-Delapierre, *Chem. Mater.*, 2003, **15**, 1993–1999.
84. A. Sárkány, I. Sajó, P. Hargittai, Z. Papp and E. Tombácz, *Appl. Catal. A: Gen.*, 2005, **293**, 41–48.
85. S. Remita, G. Picq, J. Khatouri and M. Mostafavi, *Radiat. Phys. Chem.*, 1999, **54**, 463–473.
86. J. Belloni, M. Mostafavi, H. Remita, J. L. Marignier and M. O. Delcourt, *New J. Chem.*, 1998, **22**, 1239−1255.
87. J. Belloni, *Catal. Today*, 2006, **113**, 141–156.
88. E. Gachard, J. Belloni and M. A. Subramanian, *J. Mater. Chem.*, 1996, **6**, 867–870.
89. S. Thomas, P. Bazin, L. Lakiss, V. de Waele and S. Mintova, *Langmuir*, 2011, **27**, 14689–14695.
90. S. Remita, P. Fontaine, C. Rochas, F. Muller and M. Goldmann, *Eur. Phys. J. D*, 2005, **34**, 231–233.
91. Q. Chen, X. Shen and H. Gao, *Adv. Colloid Interface Sci.*, 2010, **159**, 32–44.
92. T. I. Sutherland, C. J. Sparks, J. M. Joseph, Z. Wang, G. Whitaker, T. K. Sham and J. C. Wren, *Phys. Chem. Chem. Phys.*, 2016, **19**, 695–708.
93. P. A. Yakabuskie, J. M. Joseph, P. Keech, G. A. Botton, D. Guzonas and J. C. Wren, *Phys. Chem. Chem. Phys.*, 2011, **13**, 7198–7206.
94. A. Abedini, A. R. Daud, M. A. Abdul Hamid and N. Kamil Othman, *PLOS ONE*, 2014, **9**, e90055.
95. L. M. Alrehaily, J. M. Joseph, M. C. Biesinger, D. A. Guzonas and J. C. Wren, *Phys. Chem. Chem. Phys.*, 2013, **15**, 1014–1024.
96. L. M. Alrehaily, J. M. Joseph and J. C. Wren, *Phys. Chem. Chem. Phys.*, 2015, **17**, 24138–24150.
97. L. M. Alrehaily, J. M. Joseph, A. Y. Musa, D. A. Guzonas and J. C. Wren, *Phys. Chem. Chem. Phys.*, 2013, **15**, 98–107.
98. R. Puspalata, S. Sumathi, P. Chandramohan, S. Bera, S. Rangarajan, R. Sudha, S. V. Narasimhan and S. Velmurugan, *Radiat. Phys. Chem.*, 2013, **85**, 152–160.
99. I. Lee, S.-M. Kang, S.-C. Jang, G.-W. Lee, H. E. Shim, M. Rethinasabapathy, C. Roh and Y. S. Huh, *J. Mater. Chem. A*, 2019, **7**, 1737–1748.
100. N. Zhao, J. Peng, G. Liu, Y. Zhang, W. Lei, Z. Yin, J. Li and M. Zhai, *J. Mater. Chem. A*, 2018, **6**, 18458–18468.
101. X. Fu, Y. Zhang, P. Cao, H. Ma, P. Liu, L. He, J. Peng, J. Li and M. Zhai, *Radiat. Phys. Chem.*, 2016, **123**, 79–86.
102. P. Cao, J. Peng, S. Liu, Y. Cui, Y. Hu, B. Chen, J. Li and M. Zhai, *Sci. Rep.*, 2017, **7**, 16048.
103. G.-Y. Zhao, H. Deng, N. Tyree, M. Guy, A. Lisfi, Q. Peng, J.-A. Yan, C. Wang and Y. Lan, *Appl. Sci.*, 2019, **9**, 678.
104. J. F. Felix, A. F. da Silva, S. W. da Silva, F. Qu, B. Qiu, J. Ren, W. M. de Azevedo, M. Henini and C.-C. Huang, *Nanoscale Horiz.*, 2020, **5**, 259–267.
105. J. Lee, M. J. Krupcale and P. X. L. Feng, *Appl. Phys. Lett.*, 2016, **108**, 023106.
106. B. Ozden, M. P. Khanal, J. Park, S. Uprety, V. Mirkhani, K. Yapabandara, K. Kim, M. Kuroda, M. J. Bozack, W. Choi and M. Park, *Micro Nano Lett.*, 2017, **12**, 271–274.
107. T. Vogl, K. Sripathy, A. Sharma, P. Reddy, J. Sullivan, J. R. Machacek, L. Zhang, F. Karouta, B. C. Buchler, M. W. Doherty, Y. Lu and P. K. Lam, *Nat. Commun.*, 2019, **10**, 1202.
108. R. Miao, L. Chen, L. Shao, B. Zhang and R. G. Compton, *Angew. Chem. Int. Ed.*, 2019, **58**, 12549–12552.
109. A. Bourezgui, I. Kacem, M. Daoudi and A. F. Al-Hossainy, *J. Electron. Mater.*, 2019, **49**, 1904–1921.
110. A. Sudha, T. K. Maity and S. L. Sharma, *Mater. Lett.*, 2016, **164**, 372–375.
111. D. Lestari, I. Nurhasanah and Z. Arifin, *Adv. Sci. Lett.*, 2017, **23**, 6585–6588.
112. S. K. Sen, M. Noor, M. A. Al Mamun, M. S. Manir, M. A. Matin, M. A. Hakim, S. Nur and S. Dutta, *Opt Quantum Electron.*, 2019, **51**, 82.
113. C. Liu, T. J. Hajagos, D. Kishpaugh, Y. Jin, W. Hu, Q. Chen and Q. Pei, *Adv. Funct. Mater.*, 2015, **25**, 4607–4616.
114. Manju, M. Jain, D. Sen, A. Vij and A. Thakur, *J. Phys. Chem. Solids*, 2020, **136**, 109052.
115. A. M. Al-Baradi, M. M. El-Nahass, M. M. Abd El-Raheem, A. A. Atta and A. M. Hassanien, *Radiat. Phys. Chem.*, 2014, **103**, 227–233.

View Article Online
DOI: 10.1039/D0TA06742C

116. B. Shameer Ahmed, K. Namratha, M. B. Nandaprakash, R. Somashekar and K. Byrappa, *Radiat. Eff. Defects Solids*, 2017, **172**, 257–270.
117. S. Sohrabnezhad, D. R. Ochbelagh and M. K. Biroon, *Spectrochimica Acta Part A*, 2012, **96**, 796–800.
118. S. A. Nouh and K. Benthami, *J. Vinyl Addit. Technol.*, 2018, **25**, 271–277.
119. A. Alshahrie, N. Salah and Z. H. Khan, *Mater. Express*, 2017, **7**, 189–198.
120. V. Skákalová, M. Hulman, P. Fedorko, P. Lukáč and S. Roth, *AIP Conference Proceedings*, 2003, **685**, 143–147.
121. J. Guo, Y. Li, S. Wu and W. Li, *Nanotechnology*, 2005, **16**, 2385–2388.
122. M. Hulman, V. Skákalová, S. Roth and H. Kuzmany, *J. Appl. Phys.*, 2005, **98**.
123. S. Chen, G. Wu, Y. Liu and D. Long, *Macromolecules*, 2006, **39**, 330-334.
124. S. Gao, L. Zhu, L. Liu, A. Gao, F. Liao and M. Shao, *Electrochim. Acta*, 2016, **191**, 908–915.
125. M. Kim, S. C. Mun, C. S. Lee, M. H. Lee, Y. Son and O. O. Park, *Carbon*, 2011, **49**, 4024–4030.
126. M. H. Miao, S. C. Hawkins, J. Y. Cai, T. R. Gengenbach, R. Knott and C. P. Huynh, *Carbon*, 2011, **49**, 4940–4947.
127. Z. Xu, L. Chen, L. Liu, X. Wu and L. Chen, *Carbon*, 2011, **49**, 350–351.
128. Z. Xu, C. Min, L. Chen, L. Liu, G. Chen and N. Wu, *J. Appl. Phys.*, 2011, **109**, 054303.
129. R. C. Walker, T. Shi, E. C. Silva, I. Jovanovic and J. A. Robinson, *Phys. Status Solidi A*, 2016, **213**, 3065–3077.
130. A. Ansón-Casaos, J. A. Puértolas, F. J. Pascual, J. Hernández-Ferrer, P. Castell, A. M. Benito, W. K. Maser and M. T. Martínez, *Appl. Surf. Sci.*, 2014, **301**, 264–272.
131. J. S. Cho, W. Jang, S. C. Mun, M. Yi, J. H. Park and D. H. Wang, *Carbon*, 2018, **139**, 564–571.
132. T. Zhang, T. Wang, Y. Guo, Y. Zhai, A. Xiang, X. Ge, X. Kong, H. Xu and H. Ji, *Sci. China Mater.*, 2018, **61**, 1596–1604.
133. B. Zhang, L. Li, Z. Wang, S. Xie, Y. Zhang, Y. Shen, M. Yu, B. Deng, Q. Huang, C. Fan and J. Li, *J. Mater. Chem.*, 2012, **22**, 7775–7781.
134. Y. Zhang, H.-L. Ma, Q. Zhang, J. Peng, J. Li, M. Zhai and Z.-Z. Yu, *J. Mater. Chem.*, 2012, **22**, 13064–13069.
135. C. Yu, B. Zhang, F. Yan, J. Zhao, J. Li, L. Li and J. Li, *Carbon*, 2016, **105**, 291–296.
136. W. Chen, Z. Zhu, S. Li, C. Chen and L. Yan, *Nanoscale*, 2012, **4**, 2124–2129.
137. P. Garratt, *Polymer*, 1962, **3**, 323–334.
138. A. Chapiro, *Radiat. Phys. Chem. (1977)*, 1979, **14**, 101–116.
139. L. Chen, Z. Xu, J. Li, Y. Li, M. Shan, C. Wang, Z. Wang, Q. Guo, L. Liu, G. Chen and X. Qian, *J. Mater. Chem.*, 2012, **22**, 13460–13463.
140. C. Wang, Q. Jin, Y. Wang, H. Yin, H. Xie and R. Cheng, *Mater. Lett.*, 2012, **68**, 280–282.
141. B. Zhang, Y. Zhang, C. Peng, M. Yu, L. Li, B. Deng, P. Hu, C. Fan, J. Li and Q. Huang, *Nanoscale*, 2012, **4**, 1742–1748.
142. K. M. Aujara, B. W. Chieng, N. A. Ibrahim, N. Zainuddin and C. Thevy Ratnam, *Int. J. Mol. Sci.*, 2019, **20**, 1910.
143. G. Chen, Y. Wang, H. Weng, Z. Wu, K. He, P. Zhang, Z. Guo and M. Lin, *ACS Appl. Mater. Interfaces*, 2019, **11**, 24560−24570.
144. M. J. Williamson, R. M. Tromp, P. M. Vereecken, R. Hull and F. M. Ross, *Nat. Mater.*, 2003, **2**, 532–536.
145. H. Zheng, R. K. Smith, Y. W. Jun, C. Kisielowski, U. Dahmen and A. P. Alivisatos, *Science*, 2009, **324**, 1309–1312.
146. N. Ahmad, M. Bon, D. Passerone and R. Erni, *ACS Nano*, 2019, **13**, 13333−13342.
147. S. F. Tan, G. Bisht, U. Anand, M. Bosman, X. E. Yong and U. Mirsaidov, *J. Am. Chem. Soc.*, 2018, **140**, 11680−11685.
148. N. D. Loh, S. Sen, M. Bosman, S. F. Tan, J. Zhong, C. A. Nijhuis, P. Kral, P. Matsudaira and U. Mirsaidov, *Nat. Chem.*, 2017, **9**, 77–82.
149. E. Sutter, K. Jungjohann, S. Bliznakov, A. Courty, E. Maisonhaute, S. Tenney and P. Sutter, *Nat. Commun.*, 2014, **5**, 4946.

View Article Online
DOI: 10.1039/D0TA06742C

150. N. de Jonge and F. M. Ross, *Nat. Nanotechnol.*, 2011, **6**, 695–704.
151. H. G. Liao, L. Cui, S. Whitelam and H. Zheng, *Science*, 2012, **336**, 1011–1014.
152. H. G. Liao, D. Zherebetskyy, H. Xin, C. Czarnik, P. Ercius, H. Elmlund, M. Pan, L. W. Wang and H. Zheng, *Science*, 2014, **345**, 916–919.
153. J. Hermannsdorfer, N. de Jonge and A. Verch, *Chem. Commun.*, 2015, **51**, 16393–16396.
154. J. U. Kim, S. H. Cha, K. Shin, J. Y. Jho and J. C. Lee, *J. Am. Chem. Soc.*, 2005, **127**, 9962–9963.
155. J. Gong, H. Liu, Y. Jiang, S. Yang, X. Liao, Z. Liu and S. Ringer, *Mater. Charact.*, 2015, **110**, 1–4.
156. H. Iwasaki, T. Yoshinobu and K. Sudoh, *Nanotechnology*, 2003, **14**, R55–R62.
157. E. H. Adem, D. L. Seymour and E. B. Pattinson, *Surf. Sci.*, 1984, **141**, 1–12.
158. M. R. McCartney, P. A. Crozier, J. K. Weiss and D. J. Smith, *Vacuum*, 1991, **42**, 301–308.
159. D. J. Smith, M. R. McCartney and L. A. Bursill, *Ultramicroscopy*, 1987, **23**, 299–303.
160. A. Bachmatiuk, A. Dianat, F. Ortmann, H. T. Quang, M. O. Cichocka, I. Gonzalez-Martinez, L. Fu, B. Rellinghaus, J. Eckert, G. Cuniberti and M. H. Rümmeli, *Chem. Mater.*, 2014, **26**, 4998–5003.
161. P. J. Herley and W. Jones, *Zeitschrift für Physik D Atoms,Molecules and Clusters*, 1993, **26**, 159–161.
162. K. Li and F.-S. Zhang, *J. Nanopart. Res.*, 2009, **12**, 1423–1428.
163. W. D. Pyrz, S. Park, T. Vogt and D. J. Buttrey, *J. Phys. Chem. C*, 2007, **111**, 10824–10828.
164. L. Yu, B. M. Hudak, A. Ullah, M. P. Thomas, C. C. Porter, A. Thisera, R. H. Pham, M. De Alwis Goonatilleke and B. S. Guiton, *Chem. Mater.*, 2020, **32**, 639−650.
165. M. A. Caldwell, B. Haynor, S. Aloni, D. F. Ogletree, H. S. P. Wong, J. J. Urban and D. J. Milliron, *J. Phys. Chem. C*, 2010, **114**, 22064–22068.
166. J. H. Park, H. W. Kim, H. S. Kang, Y. H. Koo and B. C. Lee, *Mater. Res. Innov.*, 2014, **18**, S2-678–S672-684.
167. F. Zhou, R. Zhou, X. Hao, X. Wu, W. Rao, Y. Chen and D. Gao, *Radiat. Phys. Chem.*, 2008, **77**, 169–173.
168. I. Călinescu, D. Martin, D. Ighigeanu, A. I. Gavrila, A. Trifan, M. Patrascu, C. Munteanu, A. Diacon, E. Manaila and G. Craciun, *Cent. Eur. J. Chem.*, 2014, **12**, 774–781.
169. S. Seino, T. Kinoshita, T. Nakagawa, T. Kojima, R. Taniguci, S. Okuda and T. A. Yamamoto, *J. Nanopart. Res.*, 2008, **10**, 1071–1076.
170. I. V. Korolkov, A. A. Mashentseva, O. Guven, Y. G. Gorin, A. L. Kozlovskiy, M. V. Zdorovets, I. S. Zhidkov and S. O. Cholach, *Mater. Chem. Phys.*, 2018, **217**, 31–39.
171. T. Y. Kim, K. Cho, W. Park, J. Park, Y. Song, S. Hong, W. K. Hong and T. Lee, *ACS Nano*, 2014, **8**, 2774–2781.
172. L. Ma, Y. Tan, M. Ghorbani-Asl, R. Boettger, S. Kretschmer, S. Zhou, Z. Huang, A. V. Krasheninnikov and F. Chen, *Nanoscale*, 2017, **9**, 11027–11034.
173. H.-P. Komsa, S. Kurasch, O. Lehtinen, U. Kaiser and A. V. Krasheninnikov, *Phys. Rev. B*, 2013, **88**, 035301.
174. Y. Choi, D. Lim, E. Oh, C. Lim and S. H. Baeck, *J. Mater. Chem. A*, 2019, **7**, 11659–11664.
175. J. P. Thiruraman, K. Fujisawa, G. Danda, P. M. Das, T. Zhang, A. Bolotsky, N. Perea-Lopez, A. Nicolai, P. Senet, M. Terrones and M. Drndic, *Nano Lett.*, 2018, **18**, 1651−1659.
176. R. Zan, Q. M. Ramasse, R. Jalil, T. Georgiou, U. Bangert and K. S. Novoselov, *ACS Nano*, 2013, **7**, 10167–10174.
177. Y. C. Lin, D. O. Dumcenco, Y. S. Huang and K. Suenaga, *Nat. Nanotechnol.*, 2014, **9**, 391–396.
178. S. Kretschmer, H. P. Komsa, P. Boggild and A. V. Krasheninnikov, *J. Phys. Chem. Lett.*, 2017, **8**, 3061−3067.
179. A. Yoshimura, M. Lamparski, N. Kharche and V. Meunier, *Nanoscale*, 2018, **10**, 2388–2397.
180. D. Tedeschi, E. Blundo, M. Felici, G. Pettinari, B. Liu, T. Yildrim, E. Petroni, C. Zhang, Y. Zhu, S. Sennato, Y. Lu and A. Polimeni, *Adv. Mater.*, 2019, **31**, 1903795.
181. D. Ugarte, *Nature*, 1992, **359**, 707–709.
182. F. Banhart and P. M. Ajayan, *Nature*, 1996, **382**, 433–435.
183. P. Wesolowski, Y. Lyutovich, F. Banhart, H. D. Carstanjen and H. Kronmüller, *Appl. Phys. Lett.*, 1997, **71**, 1948–1950.

View Article Online
DOI: 10.1039/D0TA06742C

184. Y. Zhu, T. Yi, B. Zheng and L. Cao, *Appl. Surf. Sci.*, 1999, **137**, 83–90.
185. J. Li and F. Banhart, *Nano Lett.*, 2004, **4**, 1143–1146.
186. T. D. Yuzvinsky, W. Mickelson, S. Aloni, G. E. Begtrup, A. Kis and A. Zettl, *Nano Lett.*, 2006, **6**, 2718–2722.
187. B. Peng, M. Locascio, P. Zapol, S. Li, S. L. Mielke, G. C. Schatz and H. D. Espinosa, *Nat. Nanotechnol.*, 2008, **3**, 626–631.
188. A. Kis, G. Csanyi, J. P. Salvetat, T. N. Lee, E. Couteau, A. J. Kulik, W. Benoit, J. Brugger and L. Forro, *Nat. Mater.*, 2004, **3**, 153–157.
189. M. Terrones, H. Terrones, F. Banhart, J. Charlier and P. M. Ajayan, *Science*, 2000, **288**, 1226–1229.
190. F. Banhart, J. Li and M. Terrones, *Small*, 2005, **1**, 953–956.
191. M. Terrones, F. Banhart, N. Grobert, J. C. Charlier, H. Terrones and P. M. Ajayan, *Phys. Rev. Lett.*, 2002, **89**, 075505.
192. C. D. Cress, C. M. Schauerman, B. J. Landi, S. R. Messenger, R. P. Raffaelle and R. J. Walters, *J. Appl. Phys.*, 2010, **107**.
193. M. S. Raghuveer, A. Kumar, M. J. Frederick, G. P. Louie, P. G. Ganesan and G. Ramanath, *Adv. Mater.*, 2006, **18**, 547–552.
194. Y. J. Jung, Y. Homma, R. Vajtai, Y. Kobayashi, T. Ogino and P. M. Ajayan, *Nano Lett.*, 2004, **4**, 1109–1113.
195. C. Gomez-Navarro, P. J. de Pablo, J. Gomez-Herrero, B. Biel, F. J. Garcia-Vidal, A. Rubio and F. Flores, *Nat. Mater.*, 2005, **4**, 534–539.
196. E. Akcoltekin, T. Peters, R. Meyer, A. Duvenbeck, M. Klusmann, I. Monnet, H. Lebius and M. Schleberger, *Nat. Nanotechnol.*, 2007, **2**, 290–294.
197. V. A. Basiuk, K. Kobayashi, T. Kaneko, Y. Negishi, E. V. Basiuk and J.-M. Saniger-Blesa, *Nano Lett.*, 2002, **2**, 789–791.
198. B. Khare, M. Meyyappan, M. H. Moore, P. Wilhite, H. Imanaka and B. Chen, *Nano Lett.*, 2003, **3**, 643–646.
199. A. Hashimoto, K. Suenaga, A. Gloter, K. Urita and S. Iijima, *Nature*, 2004, **430**, 870–873.
200. M. Baraket, S. G. Walton, Z. Wei, E. H. Lock, J. T. Robinson and P. Sheehan, *Carbon*, 2010, **48**, 3382–3390.
201. L. Chen, Z. Xu, J. Li, C. Min, L. Liu, X. Song, G. Chen and X. Meng, *Mater. Lett.*, 2011, **65**, 1229–1230.
202. F. Banhart, *Rep. Prog. Phys.*, 1999, **62**, 1181–1221.
203. J. Havlik, V. Petrakova, J. Kucka, H. Raabova, D. Panek, V. Stepan, Z. Zlamalova Cilova, P. Reineck, J. Stursa, J. Kucera, M. Hruby and P. Cigler, *Nat. Commun.*, 2018, **9**, 4467.
204. O. Dutuit, A. Tabche‐Fouhaile, I. Nenner, H. Frohlich and P. M. Guyon, *J. Chem. Phys.*, 1985, **83**, 584–596.
205. T. Goulet, A. Bernas, C. Ferradini and J. P. Jay-Gerin, *Chem. Phys. Lett.*, 1990, **170**, 492–496.
206. C. Fang, W. F. Li, R. S. Koster, J. Klimes, A. van Blaaderen and M. A. van Huis, *Physical Chemistry Chemical Physics*, 2015, **17**, 365–375.
207. R. A. Crowell and D. M. Bartels, *J. Phys. Chem.*, 1996, **100**, 17940–17949.
208. A. Kumar, M. Kolaski, H. M. Lee and K. S. Kim, *The Journal of Physical Chemistry A*, 2008, **112**, 5502–5508.
209. P. Suwannakham, S. Chaiwongwattana and K. Sagarik, *RSC Adv.*, 2018, **8**, 36731–36744.
210. V. Amendola and M. Meneghetti, *Phys. Chem. Chem. Phys.*, 2009, **11**, 3805–3821.
211. G. Yang, *Prog. Mater. Sci.*, 2007, **52**, 648–698.
212. J. Zhang, J. Claverie, M. Chaker and D. Ma, *ChemPhysChem*, 2017, **18**, 986−1006.
213. D. Zhang, J. Liu, P. Li, Z. Tian and C. Liang, *ChemNanoMat*, 2017, **3**, 512–533.
214. S. Reichenberger, G. Marzun, M. Muhler and S. Barcikowski, *ChemCatChem*, 2019, **11**, 4489–4518.
215. Y. Zhou, S. H. Yu, C. Y. Wang, X. G. Li, Y. R. Zhu and Z. Y. Chen, *Adv. Mater.*, 1999, **11**, 850−852.
216. K. Huang, R. Wang, H. Wu, H. Wang, X. He, H. Wei, S. Wang, R. Zhang, M. Lei, W. Guo, B. Ge and H. Wu, *J. Mater. Chem. A*, 2019, **7**, 25779–25784.

View Article Online
DOI: 10.1039/D0TA06742C

217. K. Huang, L. Zhang, T. Xu, H. Wei, R. Zhang, X. Zhang, B. Ge, M. Lei, J. Y. Ma, L. M. Liu and H. Wu, *Nat. Commun.*, 2019, **10**, 606.
218. H. Wei, K. Huang, D. Wang, R. Zhang, B. Ge, J. Ma, B. Wen, S. Zhang, Q. Li, M. Lei, C. Zhang, J. Irawan, L. M. Liu and H. Wu, *Nat. Commun.*, 2017, **8**, 1490.
219. H. Wei, H. Wu, K. Huang, B. Ge, J. Ma, J. Lang, D. Zu, M. Lei, Y. Yao, W. Guo and H. Wu, *Chem. Sci.*, 2019, **10**, 2830−2836.
220. T. F. Li, J. J. Liu, Y. Song and F. Wang, *ACS Catal.*, 2018, **8**, 8450−8458.
221. F. Möllers, H. J. Tolle and R. Memming, *J. Electrochem. Soc.*, 1974, **121**, 1160–1167.
222. B. Kraeutler and A. J. Bard, *J. Am. Chem. Soc.*, 1978, **100**, 4317–4318.
223. K. Wenderich and G. Mul, *Chem. Rev.*, 2016, **116**, 14587–14619.
224. P. Liu, Y. Zhao, R. Qin, S. Mo, G. Chen, L. Gu, D. M. Chevrier, P. Zhang, Q. Guo, D. Zang, B. Wu, G. Fu and N. Zheng, *Science*, 2016, **352**, 797−801.
225. I. V. Lightcap, T. H. Kosel and P. V. Kamat, *Nano Lett.*, 2010, **10**, 577–583.
226. H. Gu, Y. Yang, J. Tian and G. Shi, *ACS Appl. Mater. Interfaces*, 2013, **5**, 6762–6768.
227. C. Tossi, L. Hällström, J. Selin, M. Vaelma, E. See, J. Lahtinen and I. Tittonen, *J. Mater. Chem. A*, 2019, **7**, 14519–14525.
228. J. F. Fernando, M. P. Shortell, C. J. Noble, J. R. Harmer, E. A. Jaatinen and E. R. Waclawik, *ACS Appl. Mater. Interfaces*, 2016, **8**, 14271–14283.
229. C. Pacholski, A. Kornowski and H. Weller, *Angew. Chem. Int. Ed.*, 2004, **43**, 4774–4777.
230. K. X. Yao, X. Liu, L. Zhao, H. C. Zeng and Y. Han, *Nanoscale*, 2011, **3**, 4195–4200.
231. J. D. Mangadlao, P. Cao, D. Choi and R. C. Advincula, *ACS Appl. Mater. Interfaces*, 2017, **9**, 24887−24898.
232. Y. Liu, L. He, C. Xu and M. Han, *Chem. Commun.*, 2009, **43**, 6566−6568.
233. J. Lv, S. Wu, Z. Tian, Y. Ye, J. Liu and C. Liang, *J. Mater. Chem. A*, 2019, **7**, 12627–12634.
234. A. F. Zedan, S. Moussa, J. Terner, G. Atkinson and M. S. El-Shall, *ACS Nano*, 2013, **7**, 627–636.
235. Y. H. Kim, J. S. Heo, T. H. Kim, S. Park, M. H. Yoon, J. Kim, M. S. Oh, G. R. Yi, Y. Y. Noh and S. K. Park, *Nature*, 2012, **489**, 128–132.
236. M. W. Iqbal, M. Z. Iqbal, M. F. Khan, M. A. Shehzad, Y. Seo and J. Eom, *Nanoscale*, 2015, **7**, 747–757.
237. S. Yang, Y. Liu, Y. Hao, X. Yang, W. A. Goddard, 3rd, X. L. Zhang and B. Cao, *Adv. Sci.*, 2018, **5**, 1700659.
238. J. D. Blakemore, H. B. Gray, J. R. Winkler and A. M. Muller, *ACS Catal.*, 2013, **3**, 2497–2500.
239. B. M. Hunter, J. D. Blakemore, M. Deimund, H. B. Gray, J. R. Winkler and A. M. Muller, *J. Am. Chem. Soc.*, 2014, **136**, 13118–13121.
240. A. M. Morales and C. M. Lieber, *Science*, 1998, **279**, 208–211.
241. F. Mafuné, J.-y. Kohno, Y. Takeda, T. Kondow and H. Sawabe, *J. Phys. Chem. B*, 2000, **104**, 9111–9117.
242. F. Mafuné, J.-y. Kohno, Y. Takeda and T. Kondow, *J. Phys. Chem. B*, 2002, **106**, 7575–7577.
243. G. Dukovic, M. G. Merkle, J. H. Nelson, S. M. Hughes and A. P. Alivisatos, *Adv. Mater.*, 2008, **20**, 4306–4311.
244. S. Moussa, G. Atkinson, M. SamyEl-Shall, A. Shehata, K. M. AbouZeid and M. B. Mohamed, *J. Mater. Chem.*, 2011, **21**, 9608–9619.
245. C. J. Rodrigues, J. A. Bobb, M. G. John, S. P. Fisenko, M. S. El-Shall and K. M. Tibbetts, *Phys. Chem. Chem. Phys.*, 2018, **20**, 28465−28475.
246. N. Dhenadhayalan and K. C. Lin, *ACS Appl. Mater. Interfaces*, 2020, **12**, 13759−13769.
247. B. B. Rajeeva, P. Kunal, P. S. Kollipara, P. V. Acharya, M. Joe, M. S. Ide, K. Jarvis, Y. Liu, V. Bahadur, S. M. Humphrey and Y. Zheng, *Matter*, 2019, **1**, 1606–1617.
248. R. Riedel, N. Mahr, C. Yao, A. Wu, F. Yang and N. Hampp, *Nanoscale*, 2020, **12**, 3007–3018.
249. J. Tang, M. Sakamoto, H. Ohta and K. I. Saitow, *Nanoscale*, 2020, **12**, 4352–4358.
250. V. Orsi Gordo, M. A. G. Balanta, Y. Galvao Gobato, F. S. Covre, H. V. A. Galeti, F. Iikawa, O. D. D. Couto, F. Qu, M. Henini, D. W. Hewak and C. C. Huang, *Nanoscale*, 2018, **10**, 4807–4815.

View Article Online
DOI: 10.1039/D0TA06742C

251. M. Yu, F. Waag, C. K. Chan, C. Weidenthaler, S. Barcikowski and H. Tuysuz, *ChemSusChem*, 2020, **13**, 520–528.
252. A. R. Ziefuss, S. Reich, S. Reichenberger, M. Levantino and A. Plech, *Phys. Chem. Chem. Phys.*, 2020, **22**, 4993–5001.
253. W. J. Kang, C. Q. Cheng, Z. Li, Y. Feng, G. R. Shen and X. W. Du, *ChemCatChem*, 2019, **11**, 5976–5981.
254. M. R. Karim, X. Li, P. Kang, J. Randrianalisoa, D. Ranathunga, S. Nielsen, Z. Qin and D. Qian, *Adv. Optical Mater.*, 2018, **6**, 1800726.
255. C. Y. Shih, R. Streubel, J. Heberle, A. Letzel, M. V. Shugaev, C. Wu, M. Schmidt, B. Gokce, S. Barcikowski and L. V. Zhigilei, *Nanoscale*, 2018, **10**, 6900–6910.
256. H. Park, D. A. Reddy, Y. Kim, S. Lee, R. Ma and T. K. Kim, *Chem. Eur. J.*, 2017, **23**, 13112–13119.
257. T. Okamoto, T. Nakamura, K. Sakota and T. Yatsuhashi, *Langmuir*, 2019, **35**, 12123−12129.
258. P. Zuo, L. Jiang, X. Li, B. Li, P. Ran, X. Li, L. Qu and Y. Lu, *ACS Sustainable Chem. Eng.*, 2018, **6**, 7704−7714.
259. P. Ran, L. Jiang, X. Li, B. Li, P. Zuo and Y. Lu, *Small*, 2019, **15**, 1804899.
260. X. Fan, S. Zerebecki, R. Du, R. Hubner, G. Marzum, G. Jiang, Y. Hu, S. Barcikowki, S. Reichenberger and A. Eychmuller, *Angew. Chem. Int. Ed.*, 2020, **59**, 5706–5711.
261. A. R. Ziefuss, S. Barcikowski and C. Rehbock, *Langmuir*, 2019, **35**, 6630−6639.
262. R. Torres-Mendieta, D. Ventura-Espinosa, S. Sabater, J. Lancis, G. Minguez-Vega and J. A. Mata, *Sci. Rep.*, 2016, **6**, 30478.
263. J. Zhang, C. Zhang, J. Sha, H. Fei, Y. Li and J. M. Tour, *ACS Appl. Mater. Interfaces*, 2017, **9**, 26840−26847.
264. X. Han, R. Q. Ye, Y. Chyan, T. Wang, C. H. Zhang, L. L. Shi, T. Zhang, Y. Zhao and J. M. Tour, *ACS Appl. Nano Mater.*, 2018, **1**, 5053−5061.
265. M. G. John and K. M. Tibbetts, *Appl. Surf. Sci.*, 2019, **475**, 1048–1057.
266. S. Hu, K. Cheng, E. L. Ribeiro, K. Park, B. Khomami and D. Mukherjee, *Catal. Sci. Technol.*, 2017, **7**, 2074–2086.
267. A. Tymoczko, M. Kamp, O. Prymak, C. Rehbock, J. Jakobi, U. Schurmann, L. Kienle and S. Barcikowski, *Nanoscale*, 2018, **10**, 16434–16437.
268. K. Y. Niu, J. Sun and X. W. Du, *Appl. Mech. Mater.*, 2011, **110–116**, 5487–5494.
269. Y.-j. Kim, R. Ma, D. A. Reddy and T. K. Kim, *Appl. Surf. Sci.*, 2015, **357**, 2112–2120.
270. H. J. Jung and M. Y. Choi, *Appl. Surf. Sci.*, 2018, **457**, 1050–1056.
271. Y. Men, P. Li, F. Yang, G. Cheng, S. Chen and W. Luo, *Appl. Catal. B: Environ.*, 2019, **253**, 21–27.
272. S. H. Lee, H. J. Jung, S. J. Lee, J. Theerthagiri, T. H. Kim and M. Y. Choi, *Appl. Surf. Sci.*, 2020, **506**, 145006.
273. C. Zhang, P. Li, X. Wang, J. Liu, Y. Ye, Q. Chen, D. Zhang and C. Liang, *J. Colloid Interface Sci.*, 2020, **563**, 74–80.
274. P. K. Baruah, A. K. Sharma and A. Khare, *RSC Adv.*, 2019, **9**, 15124–15139.
275. H. Jiang, S. Jin, C. Wang, R. Ma, Y. Song, M. Gao, X. Liu, A. Shen, G. J. Cheng and H. Deng, *J. Am. Chem. Soc.*, 2019, **141**, 5481−5489.
276. D. A. Goncharova, T. S. Kharlamova, I. N. Lapin and V. A. Svetlichnyi, *J. Phys. Chem. C*, 2019, **123**, 21731−21742.
277. C. Meng, M. Lin, X. Sun, X. Chen, X. Chen, X. Du and Y. Zhou, *Chem. Commun.*, 2019, **55**, 2904−2907.
278. A. Chemin, J. Lam, G. Laurens, F. Trichard, V. Motto-Ros, G. Ledoux, V. Jarý, V. Laguta, M. Nikl, C. Dujardin and D. Amans, *Nanoscale Adv.*, 2019, **1**, 3963–3972.
279. J. Jian, Y. Xu, X. Yang, W. Liu, M. Fu, H. Yu, F. Xu, F. Feng, L. Jia, D. Friedrich, R. van de Krol and H. Wang, *Nat. Commun.*, 2019, **10**, 2609.
280. Y. Wu, Z. Huang, H. Jiang, C. Wang, Y. Zhou, W. Shen, H. Xu and H. Deng, *ACS Appl. Mater. Interfaces*, 2019, **11**, 44573−44581.
281. S. Guo, Y. Zhao, H. Yuan, C. Wang, H. Jiang and G. J. Cheng, *Small*, 2020, **16**, 2000749.

View Article Online
DOI: 10.1039/D0TA06742C

282. N. K. Kulachenkov, S. Bruyere, S. A. Sapchenko, Y. A. Mezenov, D. Sun, A. A. Krasilin, A. Nominé, J. Ghanbaja, T. Belmonte, V. P. Fedin, E. A. Pidko and V. A. Milichko, *Adv. Funct. Mater.*, 2020, **30**, 1908292.
283. X. Zang, C. Jian, T. Zhu, Z. Fan, W. Wang, M. Wei, B. Li, M. Follmar Diaz, P. Ashby, Z. Lu, Y. Chu, Z. Wang, X. Ding, Y. Xie, J. Chen, J. N. Hohman, M. Sanghadasa, J. C. Grossman and L. Lin, *Nat. Commun.*, 2019, **10**, 3112.
284. H. Zhang, J. Liu, Z. Tian, Y. Ye, Y. Cai, C. Liang and K. Terabe, *Carbon*, 2016, **100**, 590–599.
285. F. Davodi, E. Muhlhausen, D. Settipani, E. L. Rautama, A. P. Honkanen, S. Huotari, G. Marzun, P. Taskinen and T. Kallio, *J. Colloid Interface Sci.*, 2019, **556**, 180–192.
286. A. De Bonis, A. Santagata, A. Galasso, A. Laurita and R. Teghil, *J. Colloid Interface Sci.*, 2017, **489**, 76–84.
287. A. De Bonis, M. Curcio, A. Santagata, A. Galasso and R. Teghil, *Nanomaterials*, 2020, **10**, 145.
288. F. Davodi, E. Muhlhausen, M. Tavakkoli, J. Sainio, H. Jiang, B. Gokce, G. Marzun and T. Kallio, *ACS Appl. Mater. Interfaces*, 2018, **10**, 31300−31311.
289. W. Gao, N. Singh, L. Song, Z. Liu, A. L. Reddy, L. Ci, R. Vajtai, Q. Zhang, B. Wei and P. M. Ajayan, *Nat. Nanotechnol.*, 2011, **6**, 496–500.
290. M. F. El-Kady, V. Strong, S. Dubin and R. B. Kaner, *Science*, 2012, **335**, 1326–1330.
291. V. Strong, S. Dubin, M. F. El-Kady, A. Lech, Y. Wang, B. H. Weiller and R. B. Kaner, *ACS Nano*, 2012, **6**, 1395–1403.
292. I. H. Kim, T. H. Im, H. E. Lee, J. S. Jang, H. S. Wang, G. Y. Lee, I. D. Kim, K. J. Lee and S. O. Kim, *Small*, 2019, **15**, 1901529.
293. G. Li, W.-C. Law and K. C. Chan, *Green Chem.*, 2018, **20**, 3689–3695.
294. X. Mo, K. C. Chan and E. C. M. Tse, *Chem. Mater.*, 2019, **31**, 8230−8238.
295. P. Nayak, Q. Jiang, N. Kurra, X. Wang, U. Buttner and H. N. Alshareef, *J. Mater. Chem. A*, 2017, **5**, 20422–20427.
296. R. Ye, D. K. James and J. M. Tour, *Adv. Mater.*, 2019, **31**, 1803621.
297. X. Zang, C. Jian, S. Ingersoll, H. Li, J. J. Adams, Z. Lu, N. Ferralis and J. C. Grossman, *Sci. Adv.*, 2020, **6**, eaaz5231.
298. A. Małolepszy, S. Błonski, J. Chrzanowska-Giżyńska, M. Wojasiński, T. Płocinski, L. Stobinski and Z. Szymanski, *Appl. Phys. A*, 2018, **124**, 282.
299. N. Mas, J. L. Hueso, G. Martinez, A. Madrid, R. Mallada, M. C. Ortega-Liebana, C. Bueno-Alejo and J. Santamaria, *Carbon*, 2020, **156**, 453−462.
300. M. Green and X. Chen, *J. Materiomics*, 2019, **5**, 503–541.
301. Y. Yao, Z. Huang, P. Xie, S. D. Lacey, R. J. Jacob, H. Xie, F. Chen, A. Nie, T. Pu, M. Rehwoldt, D. Yu, M. R. Zachariah, C. Wang, R. Shahbazian-Yassar, J. Li and L. Hu, *Science*, 2018, **359**, 1489–1494.
302. Y. Yao, Z. Huang, P. Xie, L. Wu, L. Ma, T. Li, Z. Pang, M. Jiao, Z. Liang, J. Gao, Y. He, D. J. Kline, M. R. Zachariah, C. Wang, J. Lu, T. Wu, T. Li, C. Wang, R. Shahbazian-Yassar and L. Hu, *Nat. Nanotechnol.*, 2019, **14**, 851–857.
303. S. Xu, G. Zhong, C. Chen, M. Zhou, D. J. Kline, R. J. Jacob, H. Xie, S. He, Z. Huang, J. Dai, A. H. Brozena, R. Shahbazian-Yassar, M. R. Zachariah, S. M. Anlage and L. Hu, *Matter*, 2019, **1**, 759–769.
304. G. Zhong, S. Xu, M. Cui, Q. Dong, X. Wang, Q. Xia, J. Gao, Y. Pei, Y. Qiao, G. Pastel, T. Sunaoshi, B. Yang and L. Hu, *Small*, 2019, **15**, 1904881.
305. G. Zhong, S. Xu, C. Chen, D. J. Kline, M. Giroux, Y. Pei, M. Jiao, D. Liu, R. Mi, H. Xie, B. Yang, C. Wang, M. R. Zachariah and L. Hu, *Adv. Funct. Mater.*, 2019, **29**, 1904282.
306. H. Huang, S. Zhou, C. Yu, H. Huang, J. Zhao, L. Dai and J. Qiu, *Energy Environ. Sci.*, 2020, **13**, 545–553.
307. H. Fei, J. Dong, C. Wan, Z. Zhao, X. Xu, Z. Lin, Y. Wang, H. Liu, K. Zang, J. Luo, S. Zhao, W. Hu, W. Yan, I. Shakir, Y. Huang and X. Duan, *Adv. Mater.*, 2018, **30**, 1802146.
308. Y. Zhu, S. Murali, M. D. Stoller, A. Velamakanni, R. D. Piner and R. S. Ruoff, *Carbon*, 2010, **48**, 2118–2122.
309. W. Chen, L. Yan and P. R. Bangal, *Carbon*, 2010, **48**, 1146–1152.

View Article Online
DOI: 10.1039/D0TA06742C

310. S.-H. Park, S.-M. Bak, K.-H. Kim, J.-P. Jegal, S.-I. Lee, J. Lee and K.-B. Kim, *J. Mater. Chem.*, 2011, **21**, 680–686.
311. H. Hu, Z. Zhao, Q. Zhou, Y. Gogotsi and J. Qiu, *Carbon*, 2012, **50**, 3267–3273.
312. C. H. A. Wong, O. Jankovský, Z. Sofer and M. Pumera, *Carbon*, 2014, **77**, 508–517.
313. D. Voiry, J. Yang, J. Kupferberg, R. Fullon, C. Lee, H. Y. Jeong, H. S. Shin and M. Chhowalla, *Science*, 2016, **353**, 1413–1416.
314. R. Liu, Y. Zhang, Z. Ning and Y. Xu, *Angew. Chem. Int. Ed.*, 2017, **56**, 15677-15682.

View Article Online
DOI: 10.1039/D0TA06742C

Author Biographies

Kun Guo received his Bachelor's degree in material science and engineering from Huazhong University of Science and Technology (HUST) in 2011. He obtained his Master's degree in chemical engineering from Shanghai Advanced Research Institute, Chinese Academy of Sciences in 2014 and gained his PhD degree in petroleum technology from University of Stavanger, Norway in 2018. After completing a postdoc at The University of Manchester, UK, he joined Shaoxing University as an associate professor. His research interests mainly focus on colloidal synthesis of nanomaterials, electrocatalysis and thermocatalysis.

Aliaksandr Baidak studied chemistry at the Belarusian State University, Belarus in the period of 1999–2004. He received his PhD (summa cum laude) in Natural Sciences (doctor rerum naturalium) from the University of Leipzig, Germany in 2008. After postdoc experiences in the Notre Dame Radiation Laboratory (USA), the Istituto Italiano di Tecnologia (Italy) and the University of Manchester (UK), he is now working as a Dalton Fellow at the Dalton Cumbrian Facility (DCF), the Dalton Nuclear Institute, the University of Manchester. His research focus on water radiolysis, radiation-induced degradation of ion exchange materials and organic polymers, and effects of ionizing radiation on 2D materials.

View Article Online
DOI: 10.1039/D0TA06742C

Zhixin Yu obtained his B.Sc. degree in applied chemistry from University of Science and Technology of China (USTC) in 1998, M.Sc. degree in manufacturing management from Linköping University (Sweden) in 2001, and Ph.D. degree in chemical engineering from Norwegian University of Science and Technology (Norway) in 2005. He joined the University of Stavanger (Norway) as professor in Natural Gas Technology in 2013. His main research interests include nanomaterials and nanotechnology for petroleum and clean energy production, nanocatalysis, syngas and H_2 production, biogas production, CO_2 conversion and utilization, etc.

View Article Online
DOI: 10.1039/D0TA06742C

1 **Table of Contents**

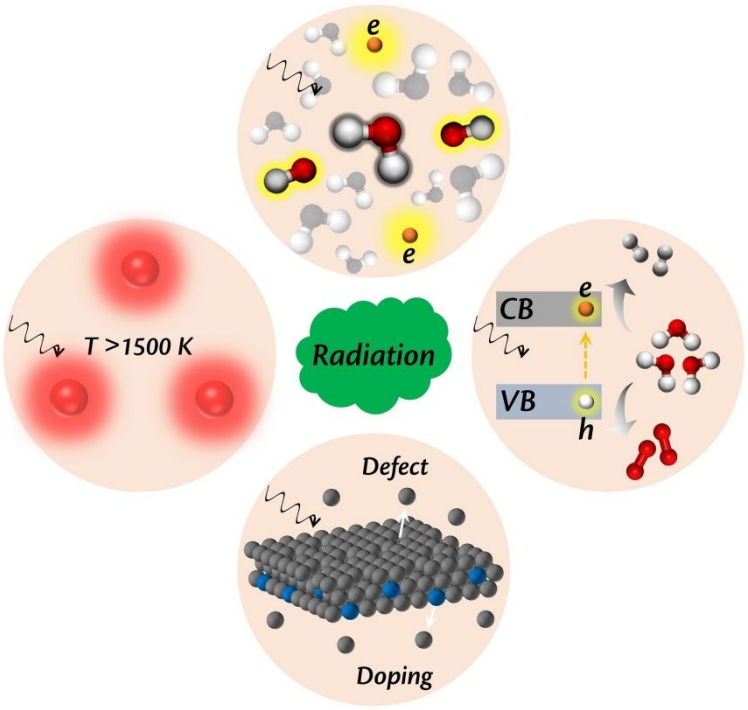

2

3 Radiation holds great potential to energize the synthesis and modification of nanomaterials with

4 high efficiency, simplicity, scalability, and environmental friendliness